Ore Geology Reviews 140 (2022) 104611

Contents lists available at ScienceDirect

Ore Geology Reviews

journal homepage: www.elsevier.com/locate/oregeorev

Mineral paragenesis and sulphide trace element distribution in the metamorphosed Lovisa Zn-Pb deposit, Bergslagen (Sweden), as revealed by 3D X-ray tomography, ore petrography and LA-ICP-MS analysis

Stefan S. Andersson [a,1,*], Fredrik Sahlström [a,b], Erik Jonsson [a,c], Stefan Luth [c], Edward P. Lynch [c], Karin Högdahl [a], Thomas Zack [d,e], Nils Gies [d], Stefan Sädbom [f], K.S. Alexander Hansson [g], Mikael Bergqvist [g]

[a] Department of Earth Sciences, Uppsala University, Villavägen 16, SE-75236 Uppsala, Sweden
[b] Department of Geosciences, UiT The Arctic University of Norway, NO-9037 Tromsø, Norway
[c] Department of Mineral Resources, Geological Survey of Sweden, Box 670, SE-75128 Uppsala, Sweden
[d] Department of Earth Sciences, University of Gothenburg, Box 460, SE-40530 Göteborg, Sweden
[e] Department of Earth Sciences, University of Adelaide, Adelaide, Australia
[f] Lovisagruvan AB, Håkansboda 1, SE-71177 Stråssa, Sweden
[g] Orexplore AB, SE-16440 Kista, Sweden

ARTICLE INFO

Keywords:
3D X-ray tomography
Sulphides
Trace elements
Ore deformation-remobilisation
Bergslagen
Sweden

ABSTRACT

This study encompasses the ore mineralogy, textures and sulphide trace element chemistry of the Palaeoproterozoic Lovisa stratiform Zn-Pb deposit and the stratigraphically underlying Lovisa Fe Formation in the Bergslagen ore province (Sweden). We investigate the relative timing of formation and subsequent modifications of its ores in relation to the c. 1.87–1.80 Ga Svecokarelian orogeny. The Lovisa Zn-Pb deposit consists of several different ore types. The massive sphalerite-galena ore is distinctly deformed, exhibiting a multiple-scale "ball ore" texture with rounded silicate clasts within a deformed, fine-grained sulphide matrix. Underlying the massive ore is a locally folded, sphalerite-rich laminated ore, interpreted to represent a metamorphosed relict primary lamination. Several generations of sphalerite-galena fracture fillings and veins occur adjacent to the main ore zones and they cross-cut early ductile structures and metamorphic features. The trace element signatures of the sphalerite-galena infillings generally mimic those of the two main ore zones, thus supporting an origin by localised remobilisation of the primary sulphide ore and demonstrating limited trace element redistribution during this process. In contrast, discrete sulphosalt-rich fracture fillings cross-cutting earlier galena-chalcopyrite-rich fracture fillings and veinlets in the Lovisa Fe Formation suggest a significant but still relatively localised redistribution of metals. Trace element mapping of sulphides from the Lovisa Zn-Pb deposit reveals that inclusion-free overgrowths on pyrite crystals are locally Co-enriched compared to the cores, which resulted from the redistribution of Co during late metamorphic processes. Combined textural and geochemical evidence suggest that the originally syngenetic exhalative sulphide ore at Lovisa was locally strongly affected by polyphase deformation and remobilisation. This was initiated during the first stage of amphibolite facies grade regional metamorphism and deformation (D_1, c. 1.87–1.85 Ga) but is mostly evident from the later stages (D_2) and the evolution to retrograde and brittle conditions (c. 1.83–1.80 Ga and later).

1. Introduction

The classic Palaeoproterozoic Bergslagen ore province in south-central Sweden hosts different styles of polymetallic sulphide and oxide deposits that show variable degrees of overprinting by polyphase metamorphism and deformation (e.g., Vivallo, 1984; Selkman, 1985; Carlon and Bleeker, 1988; Jonsson, 2004; Wagner et al., 2005; Jansson and Allen, 2015; Andersson et al., 2016; Jansson et al., 2017;

* Corresponding author.
E-mail address: stefan.andersson@geo.uu.se (S.S. Andersson).
[1] ORCID: 0000-0003-3930-440X.

https://doi.org/10.1016/j.oregeorev.2021.104611
Received 8 July 2021; Received in revised form 22 October 2021; Accepted 25 November 2021
Available online 29 November 2021

Kampmann et al., 2018). Metamorphism and deformation of sulphide ores can cause remobilisation of ore minerals and the redistribution of many major and trace elements, potentially resulting in local increases of ore grades (e.g., Wagner et al., 2007; Lockington et al., 2014; Fougerouse et al., 2016; Cugerone et al., 2020; Yu et al., 2020). So far, only a few studies have combined detailed ore textural and paragenetic studies integrated with in situ sulphide trace element analysis addressing ore and trace element distribution of deposits in the Bergslagen province (Kampmann et al., 2018, Tiu et al., 2021). Moreover, the trace elements contents of sulphides in other deposits have only been sparsely studied (e.g., Axelsson and Rodushkin, 2001; Cook et al., 2009; George et al., 2016), leaving knowledge gaps regarding the character and geochemistry of the sulphides.

This study focuses on the Lovisa Zn-Pb deposit, which is one of three base-metal sulphide deposits that are presently mined in Bergslagen (e.g., Stephens and Jansson, 2020). The Lovisa deposit has been mined intermittently since the late 1980s and is currently worked at a rate of about 40,000 tonne/year from a proven and probable reserve of 640,000 tonne of ore with 9.5 wt% Zn and 3.9 wt% Pb (Lovisagruvan AB, 2020). Until recently, studies addressing the genesis of this deposit were lacking, even though it was discovered in the 1980s during exploration for Cu-Co mineralisation in the area (Carlon, 1987; Carlon and Bleeker, 1988; Jansson et al., 2018). Following recent studies, the Lovisa deposit was concluded to represent a metamorphosed stratiform, syngenetic exhalative mineralisation exhibiting features transitional between volcanogenic massive sulphide (VMS) and sedimentary-exhalative (SEDEX)

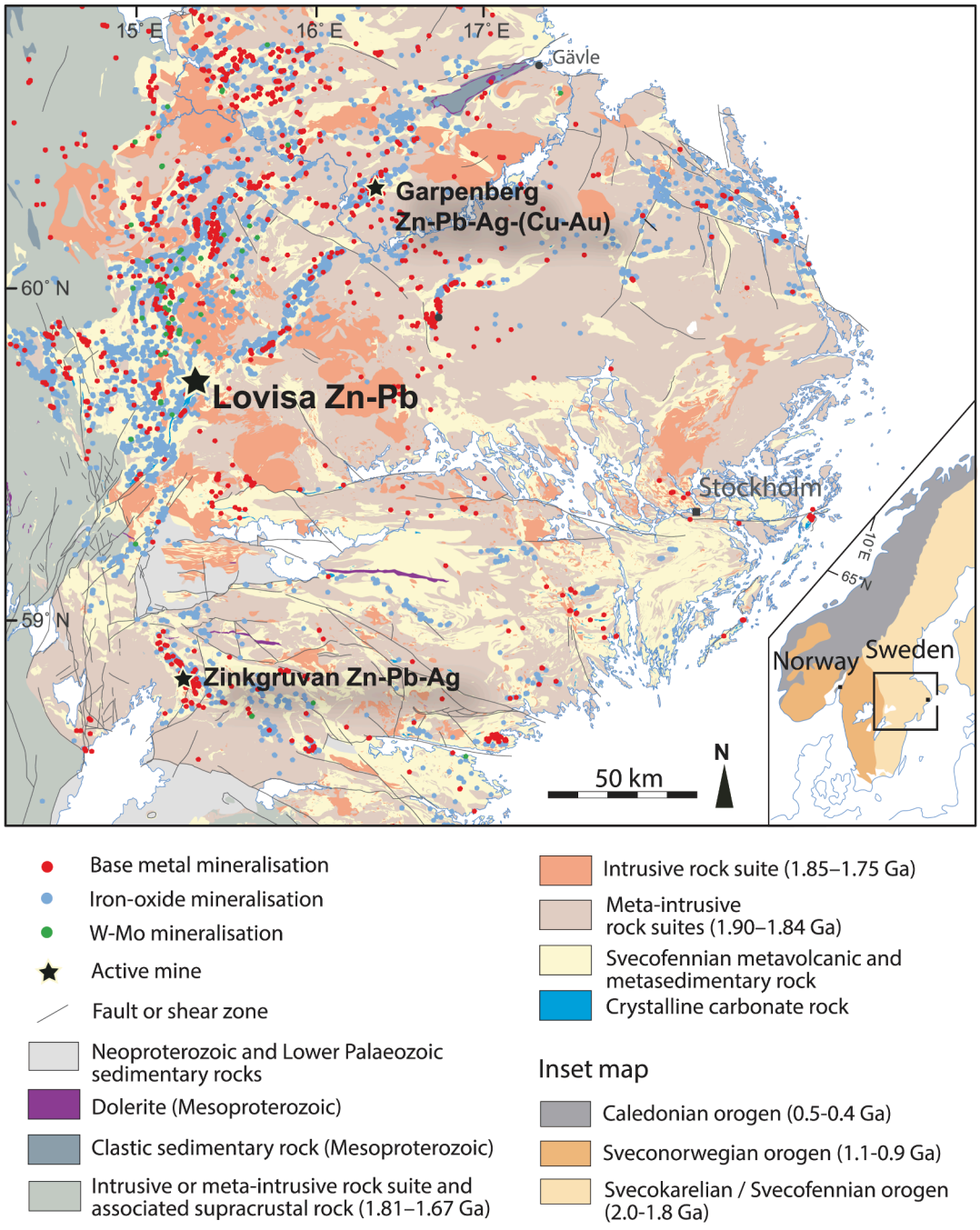

Fig. 1. Bedrock geological map of the Bergslagen ore province showing the location of the Lovisa Zn-Pb deposit. The inset figure shows a simplified geological map of the Nordic countries. Modified after Luth et al. (2019) and Stephens et al. (2009).

mineralised systems (Jansson et al., 2018; Stephens and Jansson, 2020).

The Lovisa mine is one of several active mines in Europe with ongoing testing of a new drill core scanning technique that uses concurrent 3D X-ray computed tomography and X-ray fluorescence imaging (XCT-XRF; Bergqvist et al., 2019; Sahlström et al., 2019; Cioacă et al., 2020; Munteanu et al., 2020; Luth et al., 2022). The scanning technique provides new means of imaging various ore textures, here particularly regarding the micro- to mesoscale texturally-structurally controlled metal/ore mineral distribution. The Lovisa Zn-Pb deposit is an ideal target to use this scanning technique to study the metamorphism and deformation of sulphide ores because it exhibits three distinct and texturally different ore horizons within a layered to laminated sequence, and it can be studied within a well-defined regional structural framework. Here, we integrate the results from the XCT-XRF scanning with detailed information of the ore using conventional ore and electron microscopy methods. This is, in turn, complemented by in situ trace element mineral-chemistry of the sulphide minerals using laser-ablation inductively coupled mass spectrometry (LA-ICP-MS) analysis and mapping. The combined dataset is used to investigate the mineral paragenesis and textures of the ore at Lovisa, their relative timing with regards to deformation and metamorphism, the mineral hosts for trace and critical metals, as well as the extent of trace element redistribution during remobilisation of the sulphide ore. A comparison with two deformed and metamorphosed sulphide deposits exhibiting similar features is also made, i.e., the Zn-Pb deposit in the Cinco Villas Massif, Spain (Pesquera and Velasco, 1993) and the Cu-(Zn) Matchless deposit, Namibia (Klemd et al., 1987; Cook et al., 1994).

2. Background

2.1. Regional geology

The Palaeoproterozoic Bergslagen ore province is one of the classic mining regions of Europe, featuring different types of Fe oxide and base metal sulphide deposits (Fig. 1). The Bergslagen province is located in the Svecokarelian orogen of the Fennoscandian Shield (Fig. 1; Gaal and Gorbatschev, 1987; Weihed et al., 2005; Stephens et al., 2009) and mostly comprises older (1.89–1.87 Ga) granitoids that intruded a > 1.91–1.88 Ga Svecofennian metasupracrustal succession. This metasupracrustal succession consists of mainly felsic metavolcanoclastic and metasedimentary units that were deposited in a shallow marine environment within a continental back-arc extensional setting (Allen et al., 1996; Stephens et al., 2009; Stephens and Jansson, 2020).

Most of the base-metal sulphide deposits are hosted within the stratigraphically upper part of this metasupracrustal succession and have been divided into syn- to post-volcanic seafloor exhalative (or stratiform ash-siltstone-hosted; “SAS type” in the sense of Allen et al., 1996) and subseafloor replacement (or stratabound, volcanic-associated, limestone-skarn-hosted; “SVALS type”; Allen et al., 1996) deposits. The metasupracrustal succession, including the majority of ore deposits, as well as the older granitoids, were subsequently affected by regional polyphase ductile deformation and mainly low-pressure amphibolite facies metamorphism at c. 1.87–1.80 Ga during the Svecokarelian orogeny (e.g., Stephens et al., 2009). The first phase of deformation (hereinafter referred to as D_1) in Bergslagen, which resulted in regional tectonic foliation (S_1) development locally associated with tight to isoclinal folds, is constrained to c. 1.87–1.85 Ga, slightly predating regional M_1 peak metamorphism (Hermansson et al., 2008; Johansson and Stephens, 2017; Stephens and Jansson, 2020). The second phase of deformation (D_2) is associated with regional-scale folding with axial surfaces tracing roughly NE-SW to E-W in the central parts and WNW-ESE to NW-SE in the northern and southern parts of the province. The regional-scale D_2 folding developed an axial surface foliation (S_2) and deformed the earlier S_1 foliation, which locally is transposed into S_2 (Stephens and Jansson, 2020). The timing of this phase is less well constrained but is inferred to be broadly coeval with regional M_2 metamorphism at c. 1.83–1.8 Ga, which is most conspicuous in the southern- and northernmost parts of the province where the metamorphic grade reached upper amphibolite to granulite facies (Andersson et al., 2006; Stephens and Andersson, 2015; Stephens and Jansson, 2020). A younger phase of open folding (D_3) with steep axial surfaces tracing NNW-SSE to N-S affected the western parts of the province locally (Stephens and Jansson, 2020). Younger, c. 1.85–1.75 Ga intrusive suites are synchronous with or post-date the different stages of Svecokarelian ductile deformation and metamorphism (Fig. 1; e.g., Stephens et al., 2009).

2.2. Local geology and the Lovisa Zn-Pb deposit

On a regional scale, the Lovisa Zn-Pb deposit is located on the western limb of the NE-SW striking Guldsmedshyttan syncline, which is locally overturned and has a steeply SE-dipping axial plane (Fig. 2). At Lovisa, the fold limb is in turn folded by the roughly N-S striking and SSW-plunging parasitic Lovisa anticline (Lundström, 1983; Carlon and Bleeker, 1988; Jansson et al., 2018; Luth and Bergman, 2020; Stephens and Jansson, 2020; Luth et al., 2022). The Guldsmedshyttan synclinal structure hosts several mineral deposit types in the area, including stratiform Zn-Pb deposits (e.g., Lovisa and Guldsmedshyttan), banded iron formations (BIFs; e.g., Stråssa and Blanka), skarn-hosted Fe oxide deposits (e.g., Lekeberg), and carbonate-hosted Cu-Co deposits (Fig. 2; e.g., Håkansboda; Geijer and Magnusson, 1944; Jansson et al., 2018). In a recent interpretation, the development of the Guldsmedshyttan syncline, along with the parasitic Lovisa anticline, has been attributed to non-coaxial ductile shearing associated with partitioned SE-side-up movements and sinistral slip during regional D_2 deformation, which folded the original layering (S_0) and the tectonic S_1 foliation (Luth et al., 2019, 2022; Luth and Bergman, 2020). This movement occurred along the crustal-scale so-called Western Bergslagen Boundary Zone (WBBZ; Beunk and Kuipers, 2012). Smaller asymmetric S- or Z-folds with fold axes typically plunging steeply to the SE formed synchronously with progressive D_2 shearing (Luth et al., 2022). Folds with NNW- to NW-trending steep axial surfaces with hook-like features in map view in the Håkansboda area east of Lovisa (hinge area of the Guldsmedshyttan syncline) formed through local refolding during D_3 (Fig. 2; Carlon and Bleeker, 1988; Jansson et al., 2018; Luth et al., 2022). In the vicinity of the Lovisa Zn-Pb deposit, this younger refolding phase is less apparent and the D_3 deformation is typically manifested as NW-trending faults and fractures with displacements generally<1 m. Faults with larger displacements mostly post-date D_3 deformation and includes the roughly syn- to post-D_3 N-trending Lovisa fault, which truncates the southwestern part of the Lovisa Zn-Pb ore body, and the post-D_3 NNE-trending Engvall fault east of Lovisa (Fig. 2; cf. Jansson et al., 2018; Luth et al., 2019, 2022). Overall, the deformation phases (D_2 and D_3) have resulted in moderate to steep S- to SE-plunging ore body geometries in the Lovisa Zn-Pb deposit and nearby ore deposits.

The Lovisa deposit is hosted by the Usken formation, which comprises rhyolitic metavolcanic rocks interbedded with BIFs, calc-silicate/skarn rocks and calcitic to dolomitic marbles (Fig. 3; Carlon, 1987; Jansson et al., 2018). The immediate host rock to the Zn-Pb mineralisation is a metamorphosed rhyolitic ash-siltstone. The mineralisation occurs within a 5 to 10 m-thick stratigraphic interval. The presently mined ore consists of two separate zones within this interval; the stratigraphically upper Main Ore and the lower Sphalerite Ore (Figs. 2 and 3). The Main Ore forms an up to a 1-metre thick tabular body of massive sphalerite-galena ore with subordinate pyrite. In contrast, the Sphalerite Ore comprises an up to 0.5-metre thick discrete zone of thin sphalerite-dominated laminae intercalated with the host rocks and it is only present in the southern part of the mine. Late fracture fillings and veins of coarse-grained sphalerite and galena that cross-cut the ore horizons are locally common (Jansson et al., 2018). Located stratigraphically below the Lovisa Zn-Pb deposit, the c. 25-metre thick Mn-rich Lovisa Fe Formation consists of massive magnetite interbedded

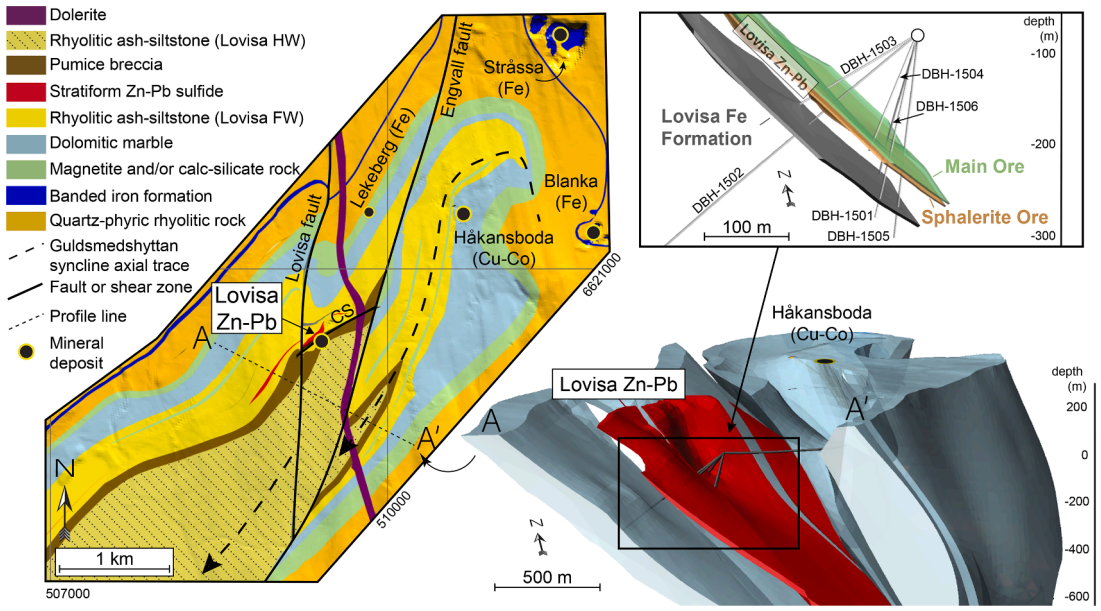

Fig. 2. Geological map of the Lovisa area within the Guldsmedshyttan syncline combined with ore models of the Lovisa Zn-Pb sulphide ore (modified after Jansson et al. (2018) and field observations made during the X-MINE project). The reference system of the map is SWEREF 99TM. The upper right model, showing the positions of the Main Ore, Sphalerite Ore and the Lovisa Fe Formation, is based on the drill core data used in this study (the 15-series). The ore geology model (red volume) is based on all available geological data, which includes historical logging data combined with geological modelling. The blue volume is marble. Modified after data from Luth et al. (2019, 2022). CS – central shear.

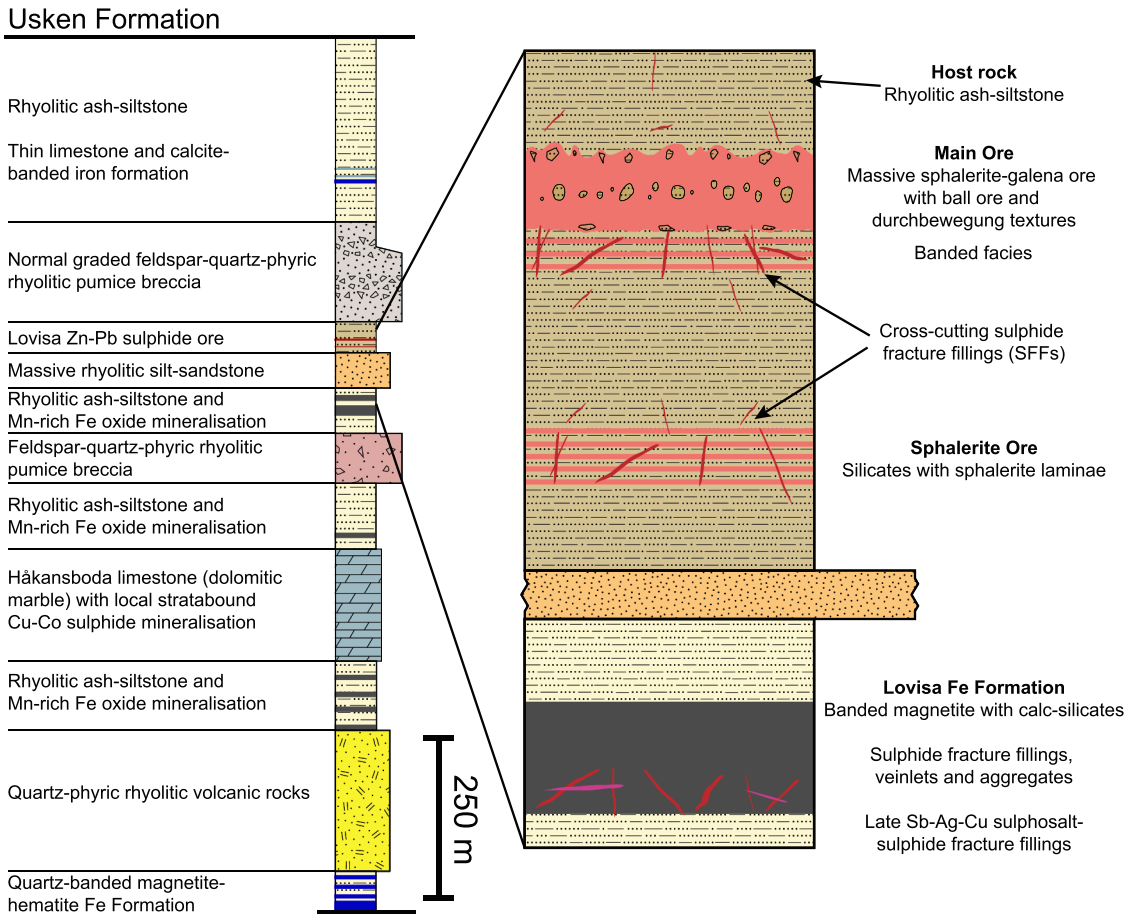

Fig. 3. A stratigraphic column of the Usken Formation hosting the Lovisa Zn-Pb sulphide ore and the underlying Lovisa Fe Formation. A close-up of the Lovisa ore zone is also shown (not completely to scale) showing the Main Ore, Sphalerite Ore and the Lovisa Fe Formation. Note that the rock terms in the column refer to the pre-metamorphic facies of the metavolcanic rocks. Modified after Jansson et al. (2018).

with calc-silicate rocks, metarhyolitic siltstones and minor dolomitic marble (Fig. 3). Within the lower part of this formation, sections of banded magnetite are associated with locally abundant sulphide assemblages (Jansson et al., 2018). The carbonate-hosted Cu-Co deposits are hosted at even lower stratigraphic levels in the Usken formation; the largest known of these is the Håkansboda Cu-Co deposit (Figs. 2 and 3; Carlon and Bleeker, 1988; Jansson et al., 2018).

3. Samples and methods

3.1. Samples

Samples were collected during the X-MINE project from drill cores that intersected the Lovisa Zn-Pb ore, the Lovisa Fe Formation and the surrounding wall rocks (drill holes/cores DBH-1501, DBH-1502, DBH-1503, DBH-1504, DBH-1505, DBH-1506; Fig. 2, Table 1). The samples were further prepared as polished thin and thick sections that were characterised as to their mineralogy and textures as well as analysed for the trace element contents of sulphides. The drill cores used in this study were not oriented.

3.2. Mineralogical and textural characterisation

The mineralogical and textural characterisation of representative ore samples were performed using reflected polarised light and electron microscopy at Uppsala University. Optical mineral identification was complemented with energy-dispersive X-ray spectrometry (EDS), summarised in the Electronic Supplementary Material (ESM).

3.3. XCT-XRF scanning

The 3D XCT-XRF drill core scanning was done using a GeoCore X10 instrument at Orexplore (Kista, Stockholm). The drill cores were scanned either as half-cores or full cores (diameter of 39 mm). Entire drill holes were scanned. The drill core pieces were assembled and placed in a sample tube and then placed vertically within the instrument. The instrument can be loaded with four separate tubes, each being 1 m long. The instrument is equipped with an X-ray source with a 50 μm focal spot size and maximal tension of 130 kVp, an X-ray spectrometer and a pixelated photon-counting transmission X-ray detector. All drill cores were scanned for 20 to 60 min per metre of drill core with a continuous rotation of the core relative to the X-ray source and detector. In principle, the X-rays emitted from the source interact with the minerals within the volume of drill core and causes the generation of characteristic and element-specific secondary X-rays (i.e., XRF) and the attenuation of X-rays, the latter depending on the chemical composition and density of the minerals as well as the energy of the X-ray source (Ketcham and Carlson, 2001; Kyle and Ketcham, 2015). For instance, galena exhibits a high attenuation because of its high density and Pb content and is easily distinguished from common gangue minerals such as quartz and feldspars containing only elements with low atomic numbers. The XCT data is used to build a 3D reconstruction of the entire drill core volume, and the combined XRF and XCT data to calculate the chemical compositions of the drill core. This calculation used stoichiometric compositions for a list of minerals specific to the Lovisa deposit as input data. The 3D reconstructions of the entire drill cores were built using cubic 3D voxels with a length of 200 μm per side. The Zn and Pb distributions and the 3D projection of minerals (attenuations) were used to

Table 1
Samples used in this study.

Sample	Type
1501–162.19–162.45	Sphalerite Ore
1501–162.80–162.95	Sphalerite Ore with sulphide fracture fillings
1502–148.21–148.32	Main Ore
1502–148.82–148.98	Main Ore
1502–148.98–149.13	Weakly laminated facies below Main Ore
1502–153.27–153.44	Sphalerite Ore with sulphide fracture fillings
1502–193.51–193.60	Lovisa Fe formation
1503–176.45–176.70	Main Ore
1503–177.35–177.48	Sulphide fracture fillings with milky quartz
1503–182.16–182.24	Sphalerite Ore
1503–201.76–201.94	Laminated facies (deeper section of the drill core)
1504–180.92–181.08	Main Ore
1504–182.10–182.25	Sulphide fracture fillings, breccia-style
1504–182.29–182.52	Sulphide fracture fillings in laminated facies below Main Ore
1504–186.80–187.05	Irregular quartz-rich sulphide fracture fillings above the Sphalerite Ore
1504–189.01–189.23	Sphalerite Ore
1505–146.73–146.90	Sulphide fracture fillings above Main Ore
1505–147.48–147.65	Main Ore with sulphide fracture fillings
1505–147.85–148.0	Sulphide fracture fillings in laminated facies below Main Ore
1505–148.55–148.65	Sulphide fracture fillings in laminated facies below Main Ore
1505–154.96–155.21	Sphalerite Ore (folded)
1505–156.20–156.55	Sphalerite Ore
1506–173.65–173.70	Skarn (green calc-silicates) with pyrite above Main Ore
1506–187.84–188.08	Main Ore
1506–188.20–188.26	Main Ore, peripheral breccia-style
1506–188.50–188.55	Main Ore, peripheral breccia-style
1506–188.91–190.00	Laminated facies below Main Ore
1506–189.51–189.60	Sulphide fracture fillings in laminated facies below Main Ore
1506–195.52–195.65	Sphalerite Ore with sulphide fracture fillings
1506–196.21–196.32	Sphalerite Ore with sulphide fracture fillings
1506–196.58–196.59	Sphalerite Ore with sulphide fracture fillings
1506–196.60–196.76	Irregular laminated facies with sulphide fracture fillings
1506–252.05–252.24	Lovisa Fe formation with late Sb-Ag-Cu-rich sulphide-sulphosalt-fluorite fracture fillings
1506–253.15–253.25	Lovisa Fe formation

The sample number represents the drill core/hole number and the drill depth of the sample (Example: for 1501–162.19–162.45, the drill core/hole is 1501 and it was sampled at 162.19 to 162.45 metres depth).

image the ore textures. The scanning data were analysed using the Insight software developed by Orexplore. In this, rotatable digital 3D volume representations of the drill cores were visualised, and characterisation of different ore textures and structures were made.

3.4. Powder X-ray diffraction analysis

Twenty samples of variably mineralised parts of the drill cores were subjected to powder X-ray diffraction (XRD) analysis at the Geological Survey of Sweden, in order to provide background and reference information to characterise the major mineralogy of the fine-grained ore and host rock assemblages. The powdered samples were run on a Siemens D-5000 automated powder diffractometer in continuous scan mode at 40 kV voltage and 40 mA current, collecting data between 2 and 65° 2-theta angles and utilising graphite-monochromated CuK_{α}-radiation. Raw data files were treated with Siemens/Bruker EVA software before manual interpretation of each file. The interpreted XRD diffractograms are available in the ESM.

3.5. Major and trace element analysis of sulphides and sulphosalts

In situ trace element mineral analysis of sphalerite, galena, pyrite, chalcopyrite, pyrrhotite and a tetrahedrite-group mineral were performed on a total of 15 ore samples using an ESI 213 NWR laser ablation system connected to an Agilent 8800QQQ inductively coupled plasma mass spectrometer in the Microgeochemistry Laboratories at the University of Gothenburg, Sweden. The instrument operates with an octopole reaction system (ORS), which is a reaction gas cell installed between two quadrupoles (Zack and Hogmalm, 2016; Hogmalm et al., 2017; König et al., 2019). By using N_2O as a reaction gas, better accuracies for several elements in the sulphides could be achieved by minimising argide, isobaric and double charged ion interferences when mass shifting elements by 16 or 32 mass units (König et al., 2019). Trace element compositions were measured over two analytical sessions. The settings were optimised for the highest sensitivity on medium mass isotopes ($^{89}Y^{16}O^{+}$). Correlations between the two sessions can be found in the ESM (Fig. S1). Elements measured were: ^{32}S (shifted to mass 64), ^{55}Mn (to mass 71), ^{56}Fe (to mass 72), ^{59}Co (to mass 75 for 1st session and on mass for 2nd session), ^{60}Ni (on mass), ^{63}Cu (on mass), ^{66}Zn (on mass), ^{71}Ga (on mass), ^{72}Ge (to mass 88), ^{75}As (to mass 91), ^{80}Se (to mass 96), ^{95}Mo (on mass), ^{107}Ag (on mass), ^{111}Cd (on mass), ^{115}In (on mass), ^{118}Sn (on mass), ^{121}Sb (on mass), ^{128}Te (to mass 144), ^{197}Au (on mass), ^{201}Hg (on mass), ^{205}Tl (on mass), ^{208}Pb (on mass), and ^{209}Bi (on mass). Laser fluence and spot sizes used during the analytical runs ranged between 4 and 5.5 J/cm^2 and 25 and 30 μm, respectively.

The reference material MASS-1 was used as an external standard for all analysed minerals, using a combination of values from Wilson et al. (2002), Danyushevsky et al. (2011) and in-house calibration. Elemental concentrations were quantified using internal standards tailored for each mineral; pyrite (stoichiometric Fe, 46.55 wt%), galena (stoichiometric Pb, 86.6 wt%), pyrrhotite (stoichiometric Fe, 62.3 wt%), sphalerite (the main cations Fe, Mn, Zn and Cd were normalised to 67.0 wt%), chalcopyrite (the two major cations Fe and Cu were normalised to 65.0 wt%), and tetrahedrite-group minerals (all cations were normalised to 16 atoms per formula unit; apfu). Data treatment and quantification of LA-ICP-MS signals were performed with the software Glitter (Griffin et al., 2008), excluding signals or segments of the signals interpreted as representing mineral inclusions. The reference materials NIST SRM 610 (Jochum et al., 2011), BAM-S005 (Yang et al., 2012), ZnS-MUL1 (Onuk et al., 2017), Po725 (Sylvester et al., 2005), Py-1 and a natural sphalerite from Bergslagen (Plåtgruvan) were measured as unknowns to evaluate the accuracy and precision. Analytical precision was almost invariably within 10% during the first session and marginally lower during the second session. External reproducibility is mostly within 20%, except for Ag and Ga (against ZnS-MUL1) and Se and Te (against NIST SRM 610), which deviate by about 20–30% relative to the reference values. Cadmium values deviate strongly and are overestimated by up to about 50%. Yet, this large deviation is rather constant over both analytical sessions and the calculated Cd concentrations of the sulphides can be readily compared within the dataset. Sulphur concentrations deviate from known reference values and have been excluded in the calculation procedures. The large deviation, particularly during the second analytical session may be related to the high volatility of S, which may cause variable Fe/S fractionation when ablating different sulphides (Gilbert et al., 2014). A detailed assessment of the data quality including the measurements of the reference materials as well the full mineral-chemical dataset is available in the ESM (Tables ESM S1-S6).

Two areas in sample 1506–187.84–188.08A (Main Ore) were selected for further element mapping by LA-ICP-MS with slightly modified conditions. The mapping was performed by ablating parallel lines across the selected areas with a constant scan direction. Spot size and spacing between the lines were set to 10 μm for map1 and 20 μm for map2 with a constant scan speed of 10 μm/s. The acquired data were processed with the Iolite Software (Paton et al., 2011). Further visualisation was optimised using MATLAB©. Results are semi-quantitative, allowing the differentiation between phases or zones with different relative concentrations of a given element.

The major element chemistry of sphalerite from a selected sample suite was also analysed by a JXA-8530F JEOL Superprobe field emission electron probe microanalysis (FE-EPMA) at the Department of Earth Sciences, Uppsala University. The analytical protocol closely followed the method of Andersson et al. (2016; beam current of 20nA, accelerating voltage of 20 kV and focused beam). Only the Fe, Zn and Cd concentrations were high enough for a comparison between LA-ICP-MS and FE-EPMA data (ESM Fig. S2).

4. Results

4.1. Ore types and their main characteristics

The ore and host rock sequence at Lovisa is characteristically layered with thicknesses of individual layers ranging from millimetre-scale laminae up to a few metre-thick beds. This structure is conspicuous throughout the ore zone, from stratigraphically above the Main Ore to below the Sphalerite Ore.

The high-grade Main Ore comprises massive sphalerite-galena-(pyrite) ore that commonly contains variably rounded, mm- to dm-sized silicate-dominated fragments (Fig. 4a-b). This ball ore texture is distinctive for the Main Ore horizon (cf. Vokes, 1969, 1973; Geijer, 1971; Carlon, 1987; Marshall and Gilligan, 1989; Jansson et al., 2018; Sahlström et al., 2019). The contacts of this ore to the host rock commonly consist of breccias infilled with sulphides. At the lower contact of the Main Ore, the massive ore transitions into a diffuse to distinctly layered texture of sulphides and silicates. Locally, the massive ore occurs adjacent to folded laminated host rock and exhibits piercement textures into the fold hinge zone that truncate and disrupt the folds (Fig. 4a). In such environments, rotated fragments of previously folded host rocks can be observed within the sulphide ore.

The zone separating the Main Ore from the Sphalerite Ore consists of a massive to weakly laminated rhyolitic metavolcanic rock that overall has a low general sulphide content, but which locally contains fracture fillings with sulphides. The Sphalerite Ore comprises fine-grained brown-beige-coloured silicates that show a distinct laminated or banded texture (Fig. 4c). The sulphides are mainly concentrated in thin laminae within the silicates (quartz, feldspars and chlorite mainly). This is particularly apparent in the 3D XCT-XRF scanning images of the Sphalerite Ore, in which sulphide minerals with a high attenuation are readily distinguished from the gangue minerals with lower attenuation (e.g., Fig. 4d-g). These sphalerite-dominated, sulphide-rich laminae are commonly folded into dm-scale parasitic folds with open to tight geometries (Fig. 4d-e). Small-scale (D_3) faulting is also prominent with displacements at the cm-scale (Fig. 4f-g). Domains with sulphide-rich

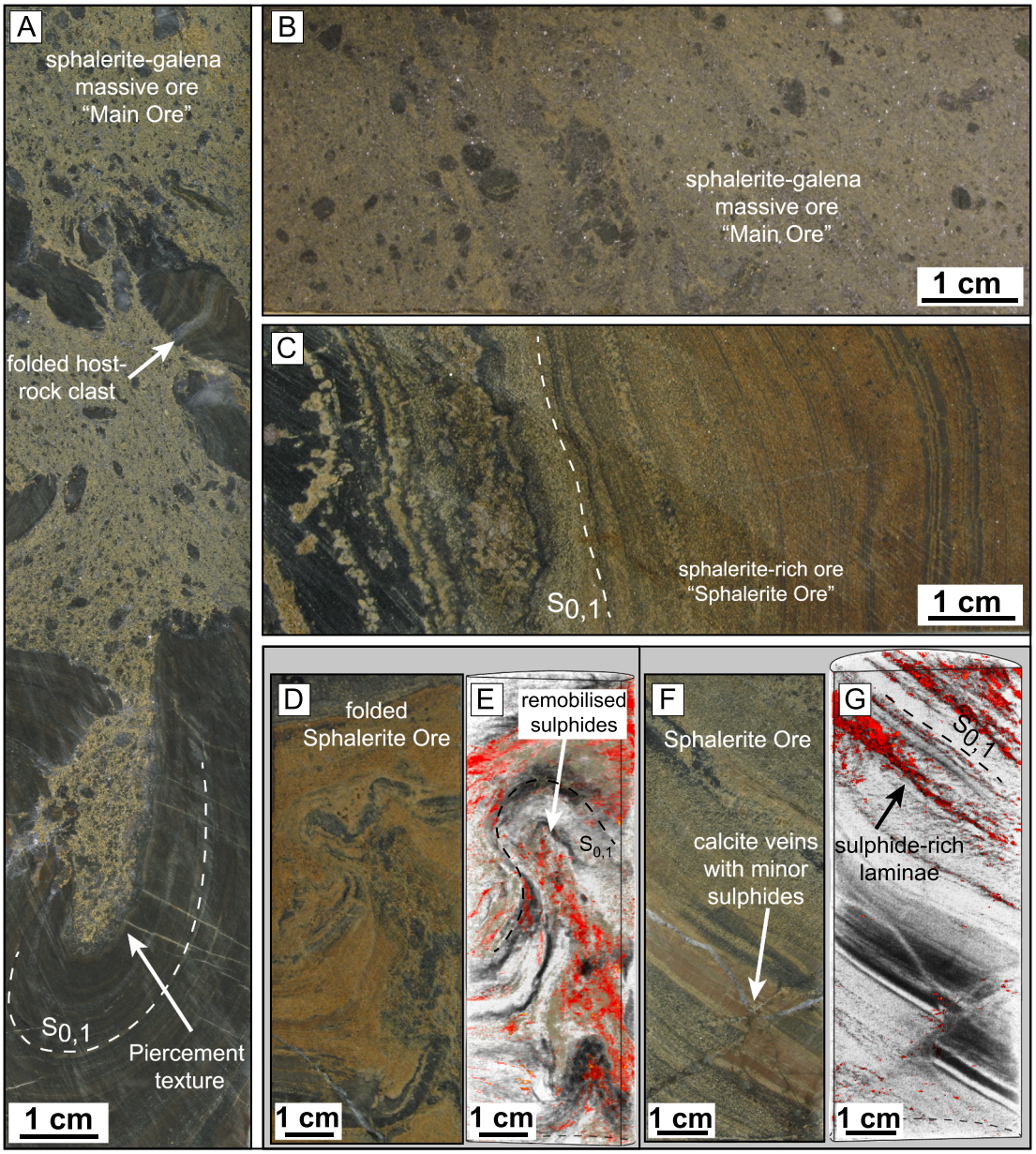

Fig. 4. A combination of photos of drill core slabs with results from the 3D XCT-XRF scans of representative ore textures from the Main Ore and Sphalerite Ore. The colours in the XCT-XRF photos represent attenuation and were adjusted separately to highlight different features in the sample. (A) Photo of the Main Ore consisting of sphalerite, galena and pyrite at the contact with the host rock showing piercement textures of sulphides flowing into an adjacent D_2 fold hinge zone truncating and disrupting the fold. The massive sulphide ore also contains partly folded fragments of the host rock. Sample 1503–176.45–176.70. (B) Photo of the Main Ore with rounded host rock fragments ("balls") within the massive sulphide ore. Sample 1506–187.84–188.08. (C) Photo showing the characteristic layering of the Sphalerite Ore. (D-E) Photo (left) and XCT-XRF scan (right) of a folded sequence of the Sphalerite Ore. From the scanning, sulphide-bearing (deep red, high attenuation) laminae can be seen tracing the fold. Sulphide-rich fracture infillings that occur within the hinge area are made visible by the scanning. Sample 1505–154.96–155.21. (F-G) Photo (left) and XCT-XRF scan (right) of a faulted sequence of the Sphalerite Ore. The faulting is associated with calcite-infilled fractures carrying minor sulphides. Sample 1503–201.76–201.94.

folded laminae similar to those in the Sphalerite Ore also occur above and below the Main Ore. Such domains are not only apparent in the immediate contact to the Main Ore but can locally be separated by intervals of more massive rhyolitic metavolcanic rocks.

Fracture fillings and veins with sulphides (hereafter termed SFF; sulphide fracture fillings) have, in contrast to previous studies (Jansson et al., 2018), been found to occur throughout the ore zone, i.e., from stratigraphically above the Main Ore to below the Sphalerite Ore (Fig. 5a-e). The SFFs are, however, more abundant close to and within the two ore horizons. The SFFs have been studied in detail using the XCT-XRF imagery, in which the 3D geometry of the SFFs is extensively visualised and their distribution and appearance can easily be used to separate them from pre-existing sulphide-rich layers. The SFFs both occur along and crosscut the primary layering and S_1 foliation, including D_2-folded sulphide-rich layers (Fig. 5a-d), and also occur in fold hinge zones (Fig. 4d-e) and associated with small-scale faults (Fig. 4f-g). Different generations of the SFFs are evidenced by cross-cutting relationships and different orientations of individual fracture fillings. However, no clear systematic relationship in terms of their mineralogy and orientation could be recognised. Thus, the SSFs could only be relatively roughly classified by their mineralogy into: 1) sphalerite-rich fracture fillings, 2) galena-rich fracture fillings, and 3) sphalerite-galena

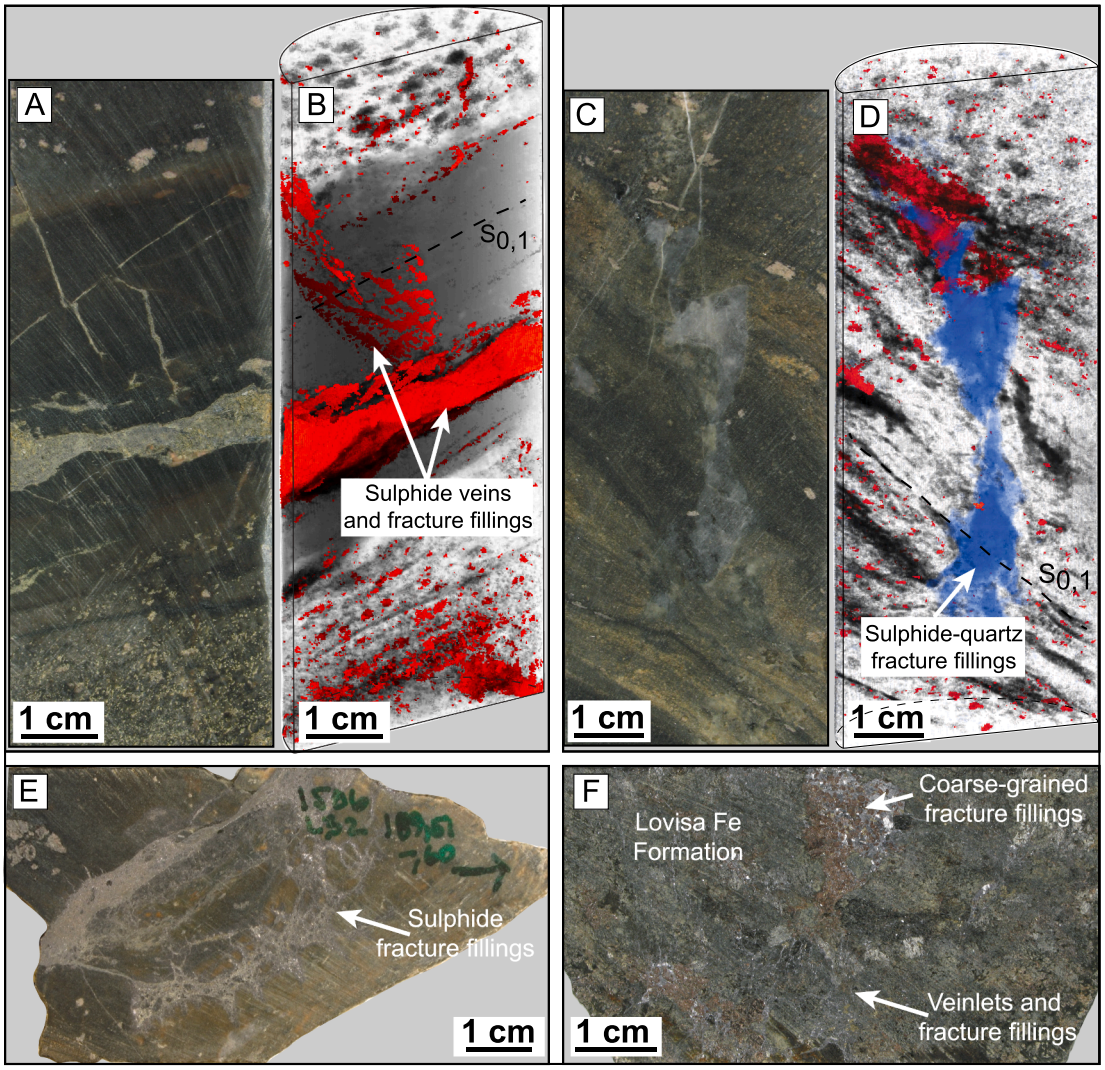

Fig. 5. A combination of photos of drill core slabs with results from the 3D XCT-XRF scans of representative ore textures from the sulphide fracture fillings (SFF) and the Lovisa Fe Formation. The colours in the XCT-XRF photos represent attenuation and were adjusted separately to highlight different features in the sample. (A-B) Photo (left) and XCT-XRF scan (right) of SFFs occurring along and cross-cutting the primary layering from a laminated sequence below the Main Ore. Sample 1504–182.29–182.52. (C-D) Photo (left) and XCT-XRF scan (right) of sulphide-rich fracture infillings associated with quartz cross-cutting the primary layering from a section just above the Sphalerite Ore. Sample 1504–186.80–187.05. (E) Photo of coarse-grained sphalerite-galena SFFs of multiple generations. Sample 1506–189.51–189.60. (F) Photo showing sulphide-rich and magnetite-bearing veinlets, fracture fillings and aggregates from the Lovisa Fe Formation. The host rock is dominated by pyrosmalite-(Fe), amphibole, biotite and garnet. Sample 1502–193.51–193.60.

fracture-fillings. The SFFs, particularly the sphalerite-rich ones, commonly contain quartz and calcite and occur in cross-cutting relationships to the $S_{0,1}$ fabric (Fig. 5c-d).

The Lovisa Fe Formation comprises massive magnetite with calc-silicates and locally abundant sulphides in the form of veinlets, fracture fillings and aggregates (Fig. 5f). These sulphide-rich assemblages are in turn crosscut by mineralogically distinct, Sb-Ag-Cu-rich sulphide-sulphosalt-fluorite fracture fillings, which have not been observed previously.

4.2. Mineralogy and textures

4.2.1. The Lovisa Zn-Pb deposit

The dominant sulphide in the Lovisa Zn-Pb deposit is sphalerite, which almost always occurs associated with galena in varying proportions. Galena is most abundant in the Main Ore and in many of the SFFs. Pyrite essentially occurs in all ore types in variable amounts, yet is never the dominant sulphide in any major assemblage. Other opaque minerals in the Lovisa Zn-Pb deposit identified in this study include chalcopyrite, magnetite, hematite and graphite, while rare arsenopyrite, chalcocite, cobaltite, molybdenite and pyrrhotite have been reported in previous unpublished studies (Zakrzewski et al., 1986, Carlon, 1987). A few isolated grains of other Ag-Sb-bearing phases and Fe-Ti-oxides were also noted in the latter studies, although it is unclear whether they were observed in the Zn-Pb deposit or the underlying Lovisa Fe Formation.

The Main Ore displays a bulk penetrative deformation fabric of the so-called Durchbewegung texture (Ramdohr, 1955; Vokes, 1973; Marshall and Gilligan, 1989), featuring coarser rounded clasts within a fine-grained, deformed groundmass dominated by sphalerite, galena and silicates (Fig. 6a-b). Milky quartz and fine-grained quartz-feldspar host rock are the main clast materials, but garnet (almandine-spessartine-grossular) and pyrite porphyroblasts have also been recognised in the form of clasts (porphyroclasts). Fine-grained aggregates of galena and silicates (mainly micas but also minor garnet) define a planar fabric, which partly or wholly wrap around larger clasts (Fig. 6a-b). Pyrite otherwise occurs as subhedral to euhedral, small crystals within sphalerite or as coarser crystals that typically exhibit inclusion-rich cores containing sphalerite, galena and silicates, and often euhedral and

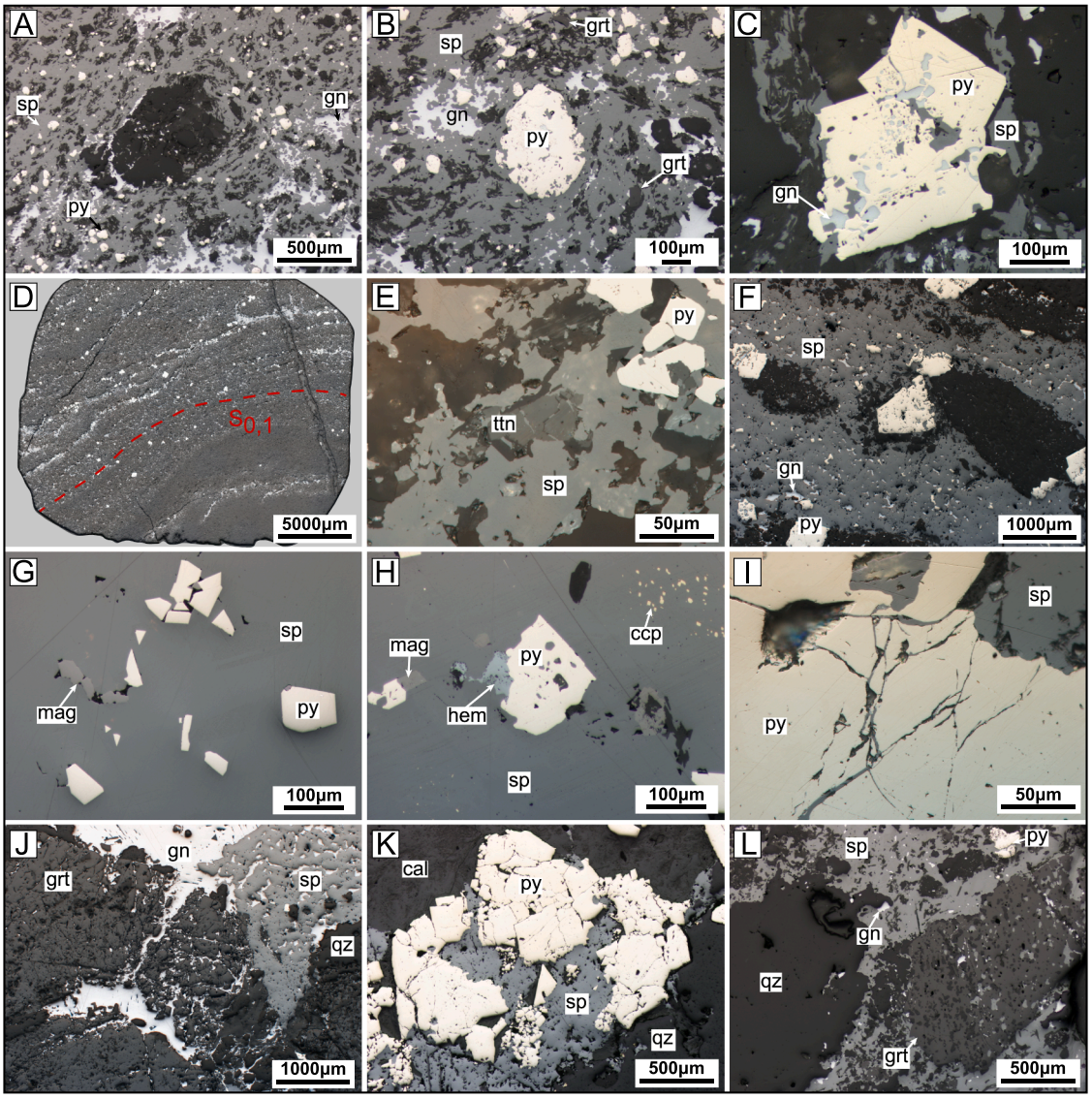

Fig. 6. Photomicrographs in reflected plane-polarised light of representative ore textures in the Lovisa Zn-Pb deposit. (A) Rounded silicate clasts within a matrix of sphalerite, galena and pyrite showing a Durchbewegung texture. Galena and smaller silicate grains are enclosing the larger clast. Main Ore (sample 1506–187.84–188.08C). (B) Rounded, relict pyrite clast within a matrix of sphalerite and galena. Smaller silicate grains, including small garnets, are wrapping around the pyrite clast. Main Ore (sample 1506–187.84–188.08C). (C) Larger pyrite crystals with inclusion-rich cores and inclusion-free overgrowths. Main Ore (sample 1506–187.84–188.08B). (D) Overview of gently folded laminated Sphalerite Ore with small sulphide-rich laminae alternating with silicate-rich laminae with disseminated sulphides. A thin calcite and sphalerite-bearing fracture crosscuts the layering. Mosaic of several photomicrographs. Sphalerite Ore (sample 1505–154.96–155.21A). (E) Close-up of the sulphide-rich laminae showing sphalerite intergrown with partly fractured titanite. Sphalerite Ore (sample 1505–154.96–155.21A). (F) Small-scale "ball ore"-type of texture in sphalerite-rich SFFs (sulphide fracture fillings) with larger incorporated silicate host-rock fragments. Pyrite is mainly occurring at intersections between sphalerite and the fragments as well as at the contact of sphalerite with the surrounding silicate gangue. Sample 1505–148.55–148.65. (G) Small, zoned euhedral pyrite crystals associated with magnetite within sphalerite-rich SFFs. Sample 1504–182.10–182.25. (H) Hematite and magnetite associated with euhedral pyrite inclusion within a sphalerite-rich SFF. Sphalerite also exhibits chalcopyrite disease. Sample 1504–182.10–182.25. (I) Large pyrite fractured and infilled by remobilised sphalerite. From a sample with SFFs just above the Sphalerite Ore (sample 1504–186.80–187.05B). (J) Large garnet porphyroblast fractured and infilled by remobilised galena. From a sample with SFFs just above the Main Ore (sample 1505–146.73–146.9). (K) Large pyrite recrystallised to smaller pyrite crystals (lower centre). From a sample with SFFs just above the Sphalerite Ore (sample 1504–186.80–187.05B). (L) Lightly fractured garnet clast with sphalerite and galena inclusions. Sample from the Main Ore (sample 1503–176.45–176.70). Abbreviations: cal – calcite, ccp – chalcopyrite, gn – galena, grt – garnet, hem – hematite, mag – magnetite, py – pyrite, sp – sphalerite, ttn – titanite, qz – quartz.

inclusion-free overgrowths (Fig. 6c). The pyrite crystals locally occur together with aggregates of galena within and around strain shadows of coarse silicate clasts. Chalcopyrite is overall rare to very rare in the Main Ore, occurring solely as minute anhedral inclusions, typically in other sulphides. Other minerals recognised in the Main Ore are chlorite, albite, K-feldspar, clinoamphibole and calcite (Jansson et al., 2018; this study).

Sphalerite is the main ore mineral in the thin sulphide-rich laminae in the Sphalerite Ore where it occurs as anhedral grains and aggregates together with minor galena and pyrite (Fig. 6d-e). Subhedral to euhedral pyrite crystals, characteristically in the form of porphyroblasts or porphyroclasts/metablasts occur mainly together with sphalerite and galena in the sulphide laminae but are also locally abundant within the surrounding silicate-rich laminae, sometimes forming distinct pyrite-dominated laminae. Similar to pyrite from the Main Ore, it typically exhibits inclusion-free overgrowths on inclusion-rich cores. Anhedral, fine-grained sphalerite and subordinate galena are also disseminated

within the silicate-rich laminae (comprised mostly of quartz, K-feldspar, albite and chlorite; Fig. 6d). Chalcopyrite is slightly more abundant in the Sphalerite Ore than in the Main Ore and is present exclusively as sparse, minute inclusions in sphalerite ('chalcopyrite disease'). Sphalerite is commonly intergrown with titanite in the sulphide laminae (Fig. 6e). Other minerals recognised in the Sphalerite Ore are clinoamphibole, muscovite, biotite, calcite, epidote, fluorapatite, clinozoisite, garnet (almandine-spessartine-grossular), zircon, ilmenite-pyrophanite solid-solutions, tourmaline and allanite-(Ce) (Jansson et al., 2018; this study).

In the SFFs, sphalerite and galena are characteristically more coarse-grained compared to the Main and Sphalerite Ores. The SFFs contain varying volumes of incorporated silicate gangue minerals, locally in the form of an indistinct ball ore texture (Fig. 6f). Sphalerite from the sphalerite-rich SFFs contains abundant subhedral to euhedral, small, and locally zoned pyrite crystals (Fig. 6g-h). Large, subhedral to euhedral blastic pyrite crystals, in turn, typically occur at the contacts between aggregates of sphalerite and the surrounding silicate gangue, or incorporated silicate gangue minerals (Fig. 6f). In galena-rich SFFs, sphalerite exhibits irregular contact relationships with galena whereas in sphalerite-rich SFFs, galena occurs as small and anhedral inclusions within the sphalerite. Compared to the other ore types, chalcopyrite is locally abundant in the SFFs, mainly occurring as rounded, randomly distributed inclusions or as elongated, probably platy inclusions in sphalerite (Fig. 6h). Coarser chalcopyrite, as compared to its occurrence as inclusions in sphalerite, typically occurs at grain boundaries between sphalerite or galena with the silicate gangue minerals. Magnetite and hematite are both closely associated with pyrite inclusions within sphalerite (Fig. 6g-h). Magnetite is also present as singular grains within sphalerite. Calcite, featuring extensive deformation twinning, typically occurs in the sphalerite-rich SFFs. Other minerals associated with the SFFs are quartz, chlorite and fluorite.

Within the entire ore zone, the large pyrite blasts are typically fractured and infilled by sphalerite and galena (Fig. 6i). The latter two minerals are also commonly present as fracture infillings in different silicate gangue minerals, including garnet porphyroblasts (Fig. 6j) and titanite (Fig. 6e). Rarely, fractured sphalerite is infilled by galena and by gangue minerals. The large pyrite porphyroblasts have locally been recrystallised into euhedral, smaller pyrite crystals (Fig. 6k). Sphalerite and galena are locally present as rare inclusions in garnet porphyroblasts (Fig. 6l).

About 15 to 20 m stratigraphically above the Main Ore, pyrite is locally associated with calc-silicate (skarn) assemblages and is texturally different from other pyrites from the Lovisa Zn-Pb ore. This pyrite occurs as coarse-grained aggregates, which are extensively fractured, and the resulting fractures have been infilled by calcite and locally chalcopyrite. Thin veinlets of remobilised pyrite emanate from the coarse-grained pyrite aggregates.

4.2.2. *Lovisa Fe Formation*

Fe-(Mn-Ca)-silicate minerals (e.g., calcic clinopyroxene, almandine-spessartine-grossular garnet, biotite and amphiboles) and magnetite are the dominant minerals in the Lovisa Fe Formation and the sulphides are only minor constituents. Nevertheless, the sulphide mineralogy in the Lovisa Fe Formation is more diverse compared to the Lovisa Zn-Pb deposit. The sulphides identified in the veinlets and fracture fillings are galena, chalcopyrite, sphalerite, pyrite and pyrrhotite. Locally, a tetrahedrite-group mineral occurs as inclusions within galena. Galena and chalcopyrite, and locally also sphalerite, pyrrhotite, pyrite and magnetite, are characteristically intergrown with micas (mainly biotite) and amphiboles (Fig. 7a) in the veinlets and fracture fillings. Magnetite is mainly present as coarse-grained aggregates and locally as euhedral crystals within galena (Fig. 7b). Both magnetite types are extensively fractured and infilled by sulphides, mainly galena. Pyrite is generally anhedral to subhedral and is intergrown with galena, with the pyrite generally exhibiting a skeletal-like habit. Such pyrite-galena intergrowths also occur as infillings in fractures in adjacent silicates (Fig. 7c).

In addition to the fracture infillings and veinlets, sphalerite also occurs together with galena, skeletal-like pyrite, pyrrhotite, magnetite

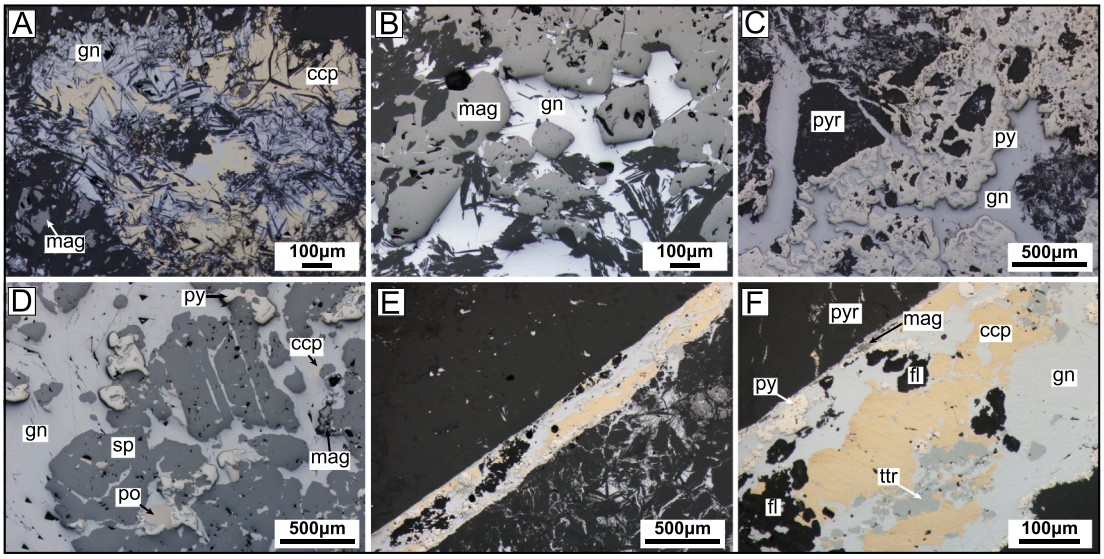

Fig. 7. Photomicrographs in reflected plane-polarised light of representative ore textures in the Lovisa Fe Formation. (A) Galena, chalcopyrite and minor magnetite intergrown with mainly acicular amphibole crystals and biotite. Sample 1506–252.05–252.24A. (B) Partly fractured anhedral magnetite with remobilised galena and euhedral magnetite (centre) within galena. Sample 1506–253.15–253.25A. (C) Galena intergrown with acicular amphibole and biotite, and skeletal-like pyrite within galena, partly also filling fractures within adjacent silicates together with galena. Sample 1506–252.05–252.24B. (D) An assemblage of galena, sphalerite, pyrite, pyrrhotite and chalcopyrite. Galena and pyrrhotite are mainly occurring along crystallographic planes within sphalerite. Chalcopyrite, pyrite and pyrrhotite are present at sphalerite grain contacts. Sample 1502–193.51–193.60. (E) Overview of the late Sb-Ag-Cu-rich sulphide and sulphosalt fracture fillings overprinting earlier galena-chalcopyrite-rich fracture fillings and veinlets (lower right). Sample 1506–252.05–252.24A. (F) Close-up of the Sb-Ag-Cu-rich fracture fillings showing chalcopyrite, galena, pyrite, tetrahedrite-group mineral (freibergite series), fluorite and small magnetite. Sample 1506–252.05–252.24A. Abbreviations: ccp – chalcopyrite, fl – fluorite, gn – galena, mag – magnetite, po – pyrrhotite, py – pyrite, pyr – pyrosmalite-(Fe), sp – sphalerite, ttr – tetrahedrite-group mineral.

Table 2
Summary of the major and trace element chemistry of sphalerite.

	Main Ore			Banded ore below Main Ore			Sphalerite Ore			Galena-sphalerite sulphide fracture fillings			Sphalerite-rich sulphide fracture fillings			Lovisa Fe Formation, fracture fillings and veinlets		
EPMA, wt%	Average	SD	n	Average	SD	n	Average	SD	n	Average	SD	n	Average	SD	n	Average	SD	n
Zn	65.75	0.35	19	N.A.			65.58	0.56	26	67.14	0.34	14	66.71	0.59	27	N.A.		
S	32.86	0.17	19	N.A.			32.54	0.25	26	32.75	0.17	14	32.91	0.17	27	N.A.		
Fe	1.90	0.10	19	N.A.			1.70	0.26	26	0.59	0.10	14	1.29	0.45	27	N.A.		
Cd	0.15	0.06	19	N.A.			0.07	0.05	17	0.22	0.07	14	*0.04*	*0.03*	8	N.A.		
Total	100.67	0.34	19	N.A.			99.86	0.55	26	100.69	0.34	14	100.93	0.30	27	N.A.		
LA-ICP-MS, ppm																		
Mn	304	38	21	139	12	10	454	308	27	143	37	5	291	70	11	1700	61	12
Fe	15,900	1730	21	13,300	849	10	16,800	5690	27	4650	1110	5	9690	2740	11	59,700	2390	12
Co	5.8	3.3	20	15	3.4	10	19	12	25	14	2.2	5	25	5.0	11	30	0.82	12
Ni	<LOD			1.3	*N < 3*		<LOD			N.A.			N.A.			<LOD		
Cu	25	10	21	58	16	10	159	233	14	82	50	5	24	11	11	43	12	12
Zn	649,000	2100	21	653,000	2410	10	650,000	5390	27	660,000	2070	5	658,000	3530	11	603,000	2610	12
Ga	*0.15*	*N < 3*		*0.073*	*0.034*	*4*	*0.084*	*0.023*	*4*	N.A.			N.A.			0.37	0.17	12
Ge	*0.18*	*0.022*	*4*	*0.43*	*N < 3*		*0.58*	*1.1*	*9*	*0.092*	*N < 3*		<LOD			*0.19*	*N < 3*	
As	*0.48*	*0.098*	*6*	N.P.			1.6	1.4	15	1.2	0.56	4	0.56	0.18	8	N.P.		
Se	*0.52*	*0.21*	*4*	<LOD			8.2	4.3	24	*0.96*	*N < 3*		1.7	0.76	11	*1.2*	*N < 3*	
Mo	*0.12*	*0.044*	*6*	N.A.			*0.23*			< LOD			*0.019*	*N < 3*		N.A.		
Ag	19	7.7	18	28	9.0	10	27	13	25	36	18	5	20	6.8	11	5.4	3.5	12
Cd	4500	354	21	3870	241	10	2600	479	27	5180	632	5	2320	82	11	5870	248	12
In	12	5.5	21	0.78	0.057	10	2.6	0.51	27	7.0	2.0	5	1.6	0.63	11	43	2.2	12
Sn	0.42	0.15	12	0.43	0.22	5	0.77	0.95	16	*0.22*	*N < 3*		1.1	1.0	6	0.3	0.16	7
Sb	1.8	1.8	17	2.9	2.2	8	5.1	3.0	24	5.3	4.0	5	1.1	0.63	11	*1.1*	*1.2*	*5*
Te	*1.0*	*0.5*	*5*	*1.1*	*N < 3*		*0.86*	*0.44*	*9*	<LOD			*0.47*	*N < 3*		*1.1*	*N < 3*	
Au	*0.013*	*0.0049*	*7*	*0.023*	*0.01*	*4*	*0.019*	*0.013*	*13*	<LOD			*0.018*	*0.0095*	*8*	*0.0093*	*N < 3*	
Hg	49	19	21	47	16	10	86	95	27	52	13	5	73	25	11	16	1.8	12
Tl	0.13	0.15	15	0.26	0.13	6	0.19	0.14	18	0.27	*N < 3*		*0.033*	*0.04*	*5*	*0.13*	*N < 3*	
Pb	*13*	*4.9*	*8*	30	8.8	6	*17*	*9.6*	*13*	38	19	4	20	14	11	4.3	2.1	10
Bi	*0.017*	*0.013*	*4*	*0.034*	*N < 3*		*0.033*	*0.043*	*9*	*0.017*	*N < 3*		0.0082	0.0045	7	*0.035*	*N < 3*	

The lower number of sample spots for some elements is because they were either, 1) not analysed (=N.A.) during the LA-ICP-MS session, 2) removed during data processing (Not present = N.P.) or, 3) is below the limit of detection (= <LOD). The listed average concentrations for the elements with low n in each ore type (marked as *italic*) should thus be considered as semi-quantitative at best because the calculated concentrations are based on only a few spots, some of which represent outliers or are close to the limit of detection. The table is based on data from the ESM, which includes documentation of all the elements.

Table 3
Summary of the major and trace element chemistry of galena.

	Main Ore			Galena-sphalerite sulphide fracture fillings			Galena-rich sulphide fracture fillings			Lovisa Fe Formation, fracture fillings and veinlets			Late Sb-Ag-Cu rich fracture fillings in Lovisa Fe Formation		
	Average	SD	n	Average	SD	n	Average	SD	n	Average	SD	n	Average	SD	n
LA-ICP-MS, ppm															
Mn	*1.2*	*2.4*	*11*				*0.12*	*N < 3*		*0.41*	*0.18*	*7*			
Fe	*1.1*	*0.87*	*4*							*0.49*	*N < 3*				
Co	0.055	0.066	7							*0.043*	*0.033*	*5*	0.063	0.03	3
Ni	*0.22*	*N < 3*								*0.21*	*N < 3*				
Cu	0.14	0.051	10	*0.093*	*N < 2*	*1*	*0.089*	*N < 3*		*0.43*	*0.65*	*5*	*7.8*	*N < 2*	
Zn	*0.55*	*N < 3*					*5.2*	*N < 3*		*0.92*	*0.83*	*5*	*8.4*	*N < 2*	
Ga	*0.019*	*0.014*	*4*				*0.032*	*N < 3*							
Ge	*0.15*	*N < 3*		*0.02*	*N < 2*	*1*				0.052	0.038	8			
As	1.1	2.4	8	0.29	*N < 2*	2				0.26	0.12	9	0.64	0.30	4
Se	2.9	2.2	23	4.0	*N < 2*	2	44	0.98	10	4.0	2.5	19	1.7	0.88	4
Mo	*0.042*	*N < 3*								*0.041*	*N < 3*		*1.2*	*N < 2*	
Ag	158	31	23	73	*N < 2*	2	555	142	10	504	190	19	1360	814	4
Cd	10	2.5	23	14	*N < 2*	2	5.4	1.4	10	51	33	19	95	42	4
In	*0.019*	*0.017*	*5*							0.083	0.073	9	0.076	0.091	3
Sn	0.14	0.16	21	*0.15*	*N < 2*	*1*	0.074	0.024	9	0.67	0.39	18	*0.29*	*N < 2*	
Sb	133	26	23	52	*N < 2*	2	405	112	10	408	183	19	895	561	4
Te	*0.32*	*0.17*	*11*				2.7	2.1	10	0.4	0.23	8	*0.52*	*N < 2*	
Au	0.014	0.013	7	0.0034	*N < 2*	2				*0.007*	*0.0043*	*5*	0.032	0.028	3
Hg	*0.55*	*N < 3*					*0.32*	*N < 3*		*0.17*	*N < 3*		*0.39*	*N < 2*	
Tl	1.2	0.25	23	0.72	*N < 2*	2	7.3	2.6	10	2.5	2.1	19	5.8	2.8	4
Pb	866,000		23	866,000		2	866,000		10	866,000		19	866,000		4
Bi	12	7.2	23	11	*N < 2*	2	199	2	10	72	65	19	20	8.5	4

Note that average concentrations for those elements with only a few numbers of spots (low n, marked as *italic*) should be considered semi-quantitative at best. See footnote of Table 2. NA = Not analysed; N.P. = Not present; <LOD = below the limit of detection.

Table 4
Summary of the major and trace element chemistry of pyrite.

	Pyrite overlying Main Ore			Main Ore			Banded ore below Main Ore			Sphalerite Ore			Sphalerite-rich sulphide fracture fillings			Lovisa Fe Formation, fracture fillings and veinlets			Late Sb-Ag-Cu rich fracture fillings in Lovisa Fe Formation		
	Average	SD	n	Average	SD	n	Average	SD	n	Average	SD	n	Average	SD	n	Average	SD	n	Average	SD	n
LA-ICP-MS, ppm																					
Mn	6.0	24	25	1.2	1.9	9	9.3	18	9	*3.5*	*N < 2*		*1.5*	*N < 2*		*1.0*	*N < 3*		0.73	0.38	3
Fe	465,000		28	465,000		14	465,000		15	465,000		3	465,000		3	465,000		10	465,000		3
Co	398	555	28	18	18	14	13	15	13	58	72	3	17	15	3	52	74	10	*0.067*	*N < 2*	
Ni	N.A.			N.A.			25	23	15	N.A.			N.A.			10	13	5	N.A.		
Cu	*0.6*	*0.65*	*13*	4.4	5.3	7	14	14	15	*1.7*	*N < 2*		129	38	3	*1.1*	*N < 3*		1480	350	3
Zn	*3.9*	*6.7*	*6*	*0.5*	*N < 3*		*7.2*	*8.3*	*4*	<LOD			N.P.			1.9	3.2	5	86	29	3
Ga	N.A.			N.A.			*0.054*	*0.058*	*4*	N.A.			N.A.			*0.033*	*N < 3*		N.A.		
Ge	*0.083*	*0.18*	*12*	0.092	0.072	8	*0.16*	*N < 3*		<LOD			*0.048*	*N < 2*		*0.033*	*N < 3*		*0.021*	*N < 2*	
As	100	144	27	402	323	14	375	184	15	1080	843	3	6640	578	3	190	318	8	67	62	3
Se	1.9	0.73	28	*0.32*	*0.18*	*5*	0.85	0.28	7	7.2	2.4	3	6.5	2.3	3	<LOD			<LOD		
Mo	0.27	0.23	19	*0.048*	*N < 3*		N.A.			*0.046*	*N < 2*		*0.07*	*N < 2*		<LOD			*0.025*	*N < 2*	
Ag	0.55	1.4	16	*1.3*	*1.8*	*4*	1.1	0.76	13	*2.5*	*N < 2*		*32*	*N < 2*		*0.42*	*N < 3*		1280	174	3
Cd	*0.088*	*0.067*	*6*	*0.1*	*N < 3*		*0.15*	*N < 3*		*0.086*	*N < 2*		N.P.			*0.19*	*0.092*	*4*	18	2.7	3
In	*0.0043*	*0.002*	*5*	*0.0081*	*N < 3*		*0.0094*	*N < 3*		*<LOD*			N.P.			*0.0082*	*0.002*	*4*	2.6	0.098	3
Sn	*0.092*	*0.032*	*10*	*0.11*	*0.057*	*4*	*0.09*	*0.054*	*5*	*0.15*	*N < 2*		*0.14*	*N < 2*		*0.079*	*N < 3*		0.21	0.034	3
Sb	1.5	3.4	25	*13*	*14*	*6*	48	43	14	*0.86*	*N < 2*		*135*	*N < 2*		*0.34*	*N < 3*		1280	167	3
Te	*0.27*	*0.038*	*4*	*0.37*	*N < 3*		0.79	0.5	9	*0.53*	*N < 2*		*0.16*	*N < 2*		*<LOD*			<LOD		
Au	*0.0036*	*0.001*	*8*	0.0069	0.0036	10	0.0085	0.0041	8	0.071	0.042	3	0.11	0.049	3	*0.0031*	*N < 3*		*0.013*	*N < 2*	
Hg	0.52	0.16	17	*0.16*	*N < 3*		*2*	*N < 3*		*0.33*	*N < 2*		<LOD			*0.89*	*N < 3*		0.62	0.25	3
Tl	*0.031*	*0.029*	*7*	0.1	0.061	11	0.56	0.93	11	0.29	0.36	3	0.3	0.32	3	*0.032*	*N < 3*		15	7.8	3
Pb	13	44	14	*86*	*69*	*4*	258	222	13	*11*	*N < 2*		*953*	*N < 2*		*3.3*	*N < 3*		248	141	3
Bi	0.016	0.025	12	0.048	0.093	9	0.4	0.36	14	0.09	0.038	3	0.14	0.044	3	0.027	0.024	6	0.0028	0.0014	3

Note that average concentrations for those elements with only a few numbers of spots (low n, marked as *italic*) should be considered semi-quantitative at best. See footnote of Table 2. NA = Not analysed; N.P. = Not present; <LOD = below the limit of detection.

Table 5
Summary of the major and trace element chemistry of chalcopyrite, freibergite series mineral and pyrrhotite.

	Lovisa Fe Formation, fracture fillings and veinlets			Late Sb-Ag-Cu rich fracture fillings in Lovisa Fe Formation			Late Sb-Ag-Cu rich fracture fillings in Lovisa Fe Formation			Lovisa Fe Formation, fracture fillings and veinlets			Lovisa Fe Formation, fracture fillings and veinlets		
	Chalcopyrite			Chalcopyrite			Freibergite			Pyrrhotite			Pyrrhotite, altered		
	Average	SD	n	Average	SD	n	Average	SD	n	Average	SD	n	Average	SD	n
LA-ICP-MS, ppm															
Mn	10	13	5	*6.1*	*N < 3*		45	34	9	4.7	1.8	5	165	16	4
Fe	309,000	4730	6	310,000	5320	12	55,800	8070	11	623,000		5	623,000		4
Co	0.12	0.025	5	0.63	1.5	10	8.2	5.8	11	62	4.8	5	153	36	4
Ni										46	7.3	5			
Cu	342,000	4970	6	340,000	5020	12	143,000	7990	11				356	209	4
Zn	236	198	6	95	37	12	9860	2810	11	*1.2*	*N < 3*		0.95	0.46	4
Ga															
Ge	*0.27*	*N < 3*		*0.088*	*N < 3*		1.0	0.81	11	*0.19*	*N < 3*		0.81	0.2	4
As	7.8	8.7	4	*0.62*	*0.44*	*4*	6.2	5.4	11	140	17	5	8.4	1.2	4
Se	*0.43*	*N < 3*		*0.66*	*0.18*	*4*	*0.26*	*N < 3*		*1.5*	*N < 3*		*0.26*	*N < 2*	
Mo				*0.37*	*N < 3*		*0.36*	*0.25*	*6*				0.5	0.49	4
Ag	202	28	6	250	48	6	349,000	22,800	11	0.98	0.43	5	802	169	4
Cd	17	8.8	6	15	3.7	11	2560	475	11	*0.072*	*N < 3*		5.6	0.96	4
In	3.8	1.6	6	3.7	0.71	12				*0.021*	*N < 3*		0.014	0.016	3
Sn	2.0	1.3	4	0.88	0.5	9	17	31	11	0.18	*N < 3*		0.12	0.061	3
Sb	13	9.6	5	27	20	6	232,000	9890	11	*0.46*	*N < 3*		1530	250	4
Te	*1.6*	*N < 3*		*1*	*0.27*	*5*	0.76	0.52	7						
Au	*0.029*	*N < 3*		0.067	0.046	9	7.6	18	10						
Hg	*0.39*	*N < 3*		*0.84*	*0.22*	*4*	0.73	0.44	9				0.61	0.2	4
Tl	1.2	1.5	6	7.3	14	10	7.2	6.0	11	*0.015*	*N < 3*		35	8.7	4
Pb	*15*	*N < 3*		40	16	6	*151*	*N < 3*		3.3	0.99	5	2840	586	4
Bi	*0.53*	*N < 3*		*0.29*	*0.37*	*5*	0.056	0.067	8	*0.044*	*N < 3*		*0.011*	*N < 2*	

Note that average concentrations for those elements with only a few numbers of spots (low n, marked as *italic*) should be considered semi-quantitative at best. See footnote of Table 2. NA = Not analysed; N.P. = Not present; <LOD = below the limit of detection.

and minor chalcopyrite in coarse aggregates with sparse silicate gangue mineral inclusions (Fig. 7d). It is characteristic of these aggregates that pyrrhotite and galena are present as inclusions in the sphalerite grains and aggregates, locally as platy crystals within the sphalerite (Fig. 7d). Chalcopyrite and skeletal-like pyrite mainly occur at galena-sphalerite contacts, locally together with pyrrhotite. Magnetite is mainly present here at the contacts between sulphide aggregates and the silicate groundmass. Pyrrhotite is locally replaced by pyrite. Other gangue minerals recognised in the Lovisa Fe Formation include pyrosmalite-(Fe), quartz, chlorite, epidote, microcline, and fluorapatite (Jansson et al., 2018; this study).

Late Sb-Ag-Cu-rich sulphide-sulphosalt-fluorite fracture fillings consist of galena, chalcopyrite, pyrite, a tetrahedrite-group mineral belonging to the freibergite series, fluorite and locally magnetite, sphalerite, pyrargyrite, calcite, chlorite and another Ag-rich phase, which due to its very small size could not be fully characterised (Fig. 7e-f). Pyrite is present as small, subhedral to euhedral crystals showing a preferred growth direction inward, towards the central part of the fractures, from the fracture substrate. Slightly larger pyrite crystals locally exhibit a sieve texture with irregular grain boundaries and with inclusions of the tetrahedrite-group mineral, galena, and fluorite. Galena, chalcopyrite, and the tetrahedrite-group mineral all exhibit anhedral morphologies towards each other. Sphalerite occurs as small (25–50 μm), rare anhedral grains within chalcopyrite.

4.3. Trace element chemistry of sulphides and sulphosalts

A summary of the trace element concentrations of sulphides from the different ore types is shown in Tables 2, 3, 4 and 5, as well as Fig. 8. The full mineral-chemical dataset is included in the ESM.

4.3.1. Sphalerite

Besides Zn and S, the main elements hosted by sphalerite are Fe, Mn and Cd (Table 2; Figs. 8 and 9). The Fe concentration is relatively low in the sphalerite from the Lovisa Zn-Pb deposit, normally below 2 wt% Fe, except in some samples from the Sphalerite Ore, which reach 3 wt%. Sphalerite from the late SFFs exhibits the overall lowest Fe concentrations, ranging from 0.3 to 1.3 wt% Fe (Fig. 9a). In contrast, sphalerite from the Lovisa Fe Formation is enriched in Fe, averaging around 6 wt% Fe. Similarly, the Mn (1500–2000 ppm) and Cd (c. 6000 ppm) concentrations are also higher compared to sphalerite from the Lovisa Zn-Pb deposit (Mn: < 500 ppm; Cd: 2000–5000 ppm; Fig. 9b).

With regards to trace elements, only Ag, Co, Cu, Hg, In and Pb exceed 10 ppm. However, micro- to nanoscale inclusions of galena in sphalerite, while not visible in the laser-ablation signals, likely contribute to higher Pb and Ag concentrations in most spots. This is corroborated by a positive correlation between Pb and Ag in sphalerite across the dataset, even after excluding analyses where Pb contributions from inclusions were apparent from the laser-ablation signals (Fig. 9c; cf. also Cook et al. 2009). Similarly, elevated Cu concentrations mostly originate from chalcopyrite inclusions in sphalerite. This is evident as the sphalerite from the Sphalerite Ore, which variably exhibits 'chalcopyrite disease', also exhibits the highest Cu concentrations (Tables 2 and ESM S1).

Sphalerite from all different ore types at Lovisa contains variable Co concentrations (Figs. 8 and 9d). Sphalerite from the Main Ore has the lowest Co concentration observed (<10 ppm), with slightly higher concentrations in the banded facies below the Main Ore. The highest Co concentration in sphalerite was found in the sphalerite-rich SFFs as well as locally within the Sphalerite Ore (up to 40 ppm Co). Indium is another element that is consistently above about 1 ppm in sphalerite. Sphalerite from the Lovisa Fe Formation has comparably higher In concentrations (40–50 ppm) relative to the Lovisa Zn-Pb ore, although sphalerite from the Main Ore locally contains up to 20 ppm In. Sphalerite from the lower breccia contact of the Main Ore trends to slightly lower In and Cd concentrations (Figs. 8 and 9a-b), similar to sphalerite from the SFFs.

As for the remaining trace elements in sphalerite, only Se concentrations are distinctly different between the ore types. Particularly, sphalerite from the Sphalerite Ore is characteristically enriched in Se (up to 15 ppm) compared to other sphalerite types, which typically have concentrations below 5 ppm (Figs. 8 and 9d). Gallium, Ge, Sn, and Tl, which are known to be hosted in sphalerite in some sulphide deposits (e.g., George et al. 2016), are all typically below 1 ppm (ESM Table S1).

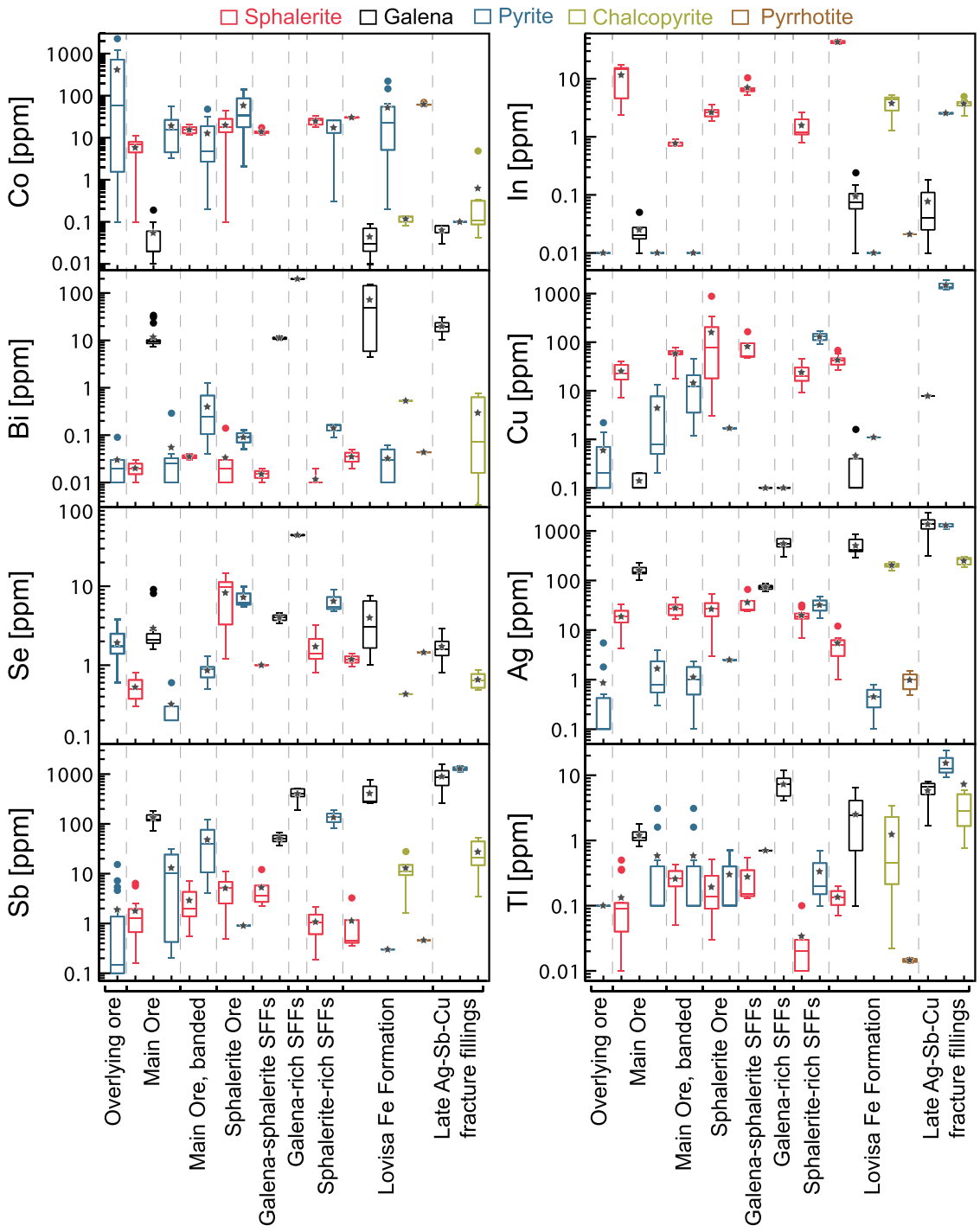

Fig. 8. Box-and-whisker plots showing the distribution of Co, In, Bi, Cu, Se, Ag, Sb and Tl between the different sulphide minerals in all ore types. The boxes outline the lower and upper quartiles of the datasets, the horizontal line the median and the whiskers the minimum and maximum values excluding the outliers, which are shown as individual symbols. The grey stars denote the averages of each type.

4.3.2. Galena

Galena in the Lovisa Zn-Pb deposit and Fe Formation typically contains elevated concentrations of Ag (80–2300 ppm), Bi (5–200 ppm) and Sb (40–1600 ppm), as well as slightly lower concentrations of Cd (4–130 ppm), Se (1–45 ppm), Te (0.1–8 ppm) and Tl (0.1–12 ppm; Table 3; Fig. 8). Locally, In and Sn reach 0.2 ppm and 1.1 ppm, respectively. The remaining elements are below or close to their limits of detection (ESM Table S2).

Galena from the Main Ore is depleted in most trace elements (e.g., Ag, Bi, and Sb) compared to galena from the other ore types (galena from the Sphalerite Ore was not analysed). Galena from the Lovisa Fe Formation, including galena in the late Sb-Ag-Cu-rich fracture fillings, contains higher concentrations of most trace elements, again most notably Ag, Bi and Sb.

Galena in the SFFs is either very low in all trace elements (galena-sphalerite SFFs) or locally shows higher concentrations of Ag (300–700 ppm; galena-rich SSFs), Bi (c. 200 ppm), Sb (200–500 ppm), Se (c. 45 ppm) and Te (2–9 ppm). Galena from the breccia-like lower contact of the Main Ore exhibits higher Bi and Se concentrations, similar to galena from the remobilised SFFs (Fig. 8; shown as outliers in the Bi and Se diagrams).

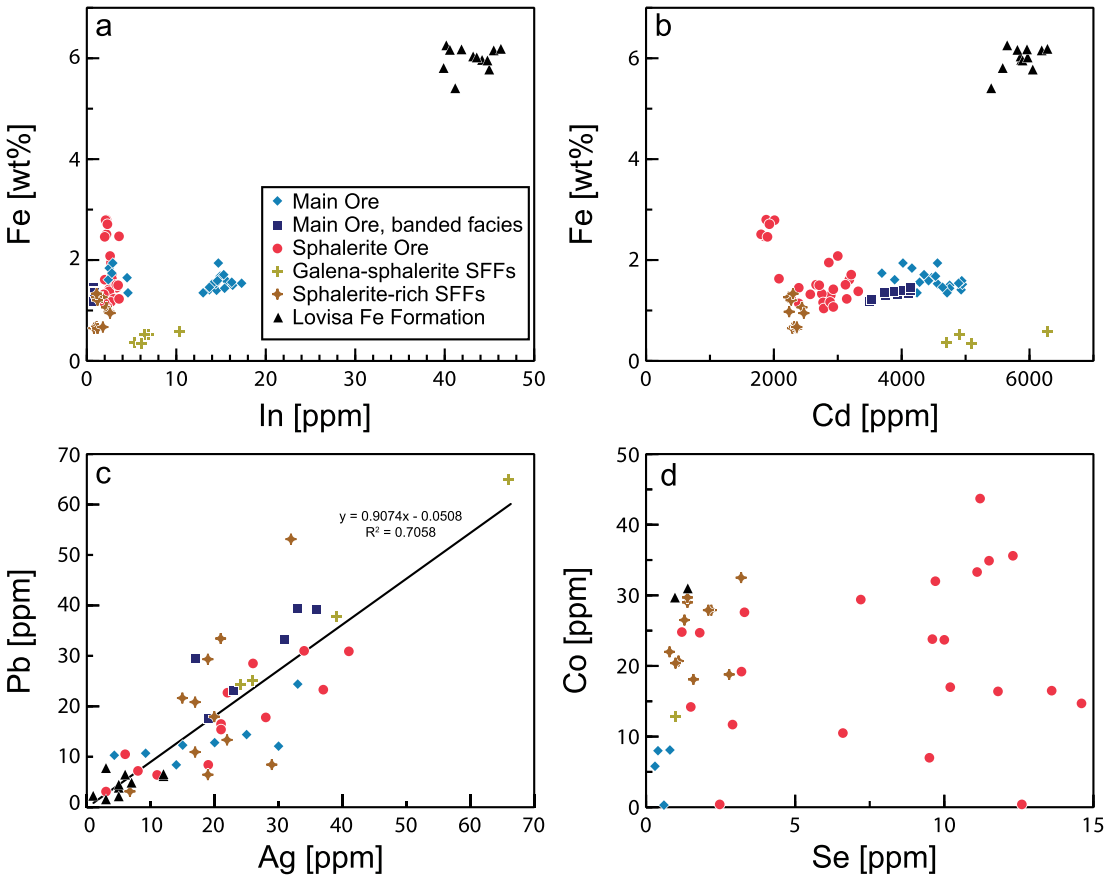

Fig. 9. Diagrams illustrating trace element concentrations in sphalerite. (A) Fe vs In. (B) Fe vs Cd. (C) Pb vs Ag. (D) Co vs Se.

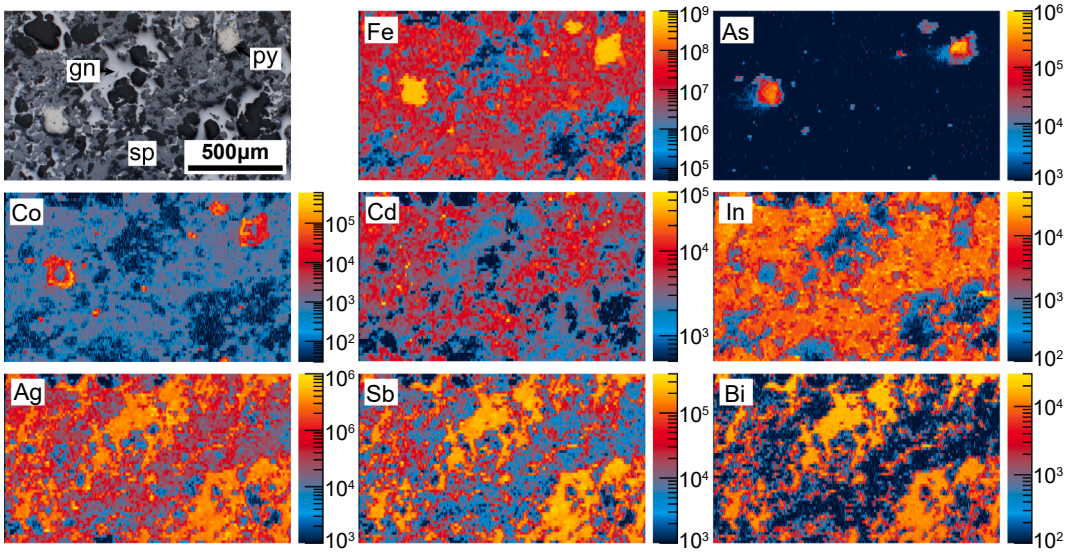

Fig. 10. Result from LA-ICP-MS scanning (map1) of a section from the Main Ore (sample 1506–187.84–188.08A). Note the Co-rich overgrowths on pyrite. The Co concentration in the overgrowths is in the order of 20–30 ppm. The scale is in counts per second.

4.3.3. Pyrite

The trace elements Au, As, Bi, Co, Mn, Ni, Sb and Se were generally present in detectable amounts in pyrite (Table 4; Fig. 8). The remaining suite of potentially expected elements (Cd, Cu, Ga, Ge, Hg, In, Mn, Pb, Sn, Te and Zn) were close to or below their limits of detection and exhibited erratic distributions (ESM Table S3). Locally high concentrations of these elements may thus be a result of the presence of micro- to nanoscale inclusions.

Of the trace elements measured, As shows the highest concentrations in pyrite. The As concentrations range from below 1 ppm to 7300 ppm and is highly variable within all ore types. The highest As concentrations were found in coarse pyrite crystals associated with the SFFs, where pyrite occurs at the contacts between the sphalerite infill and the surrounding silicate gangue (Fig. 6f). The variable As concentrations in

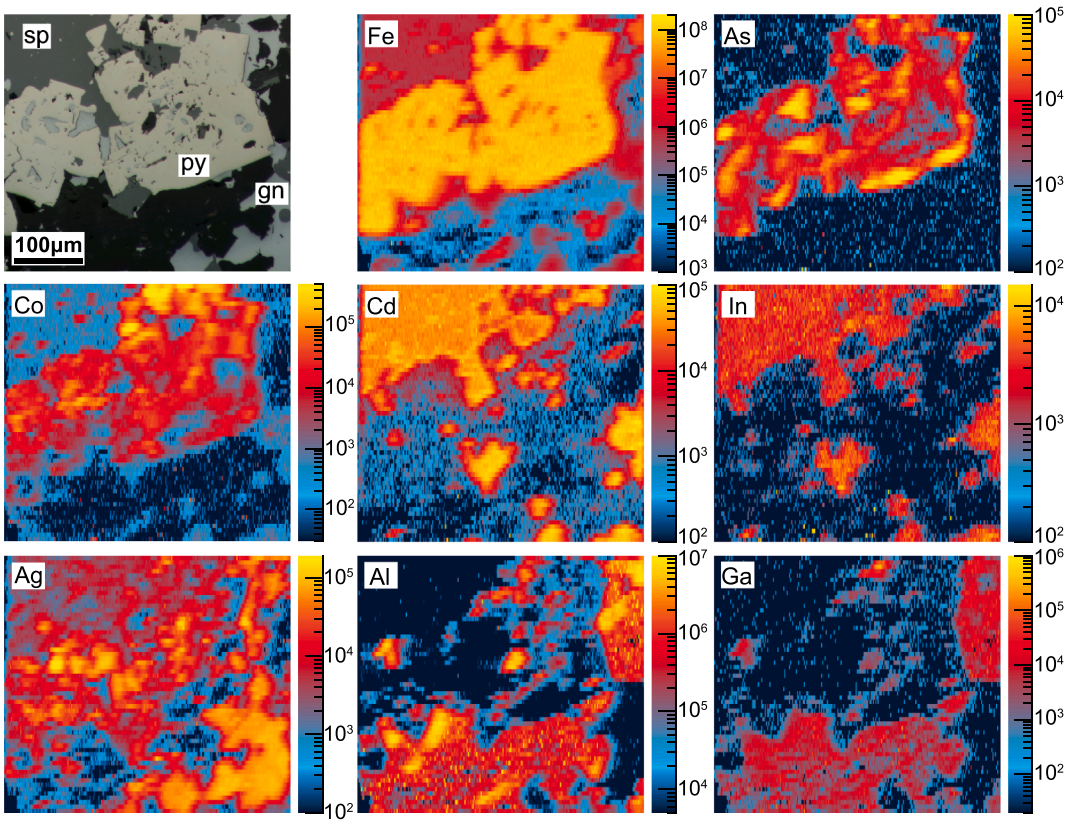

Fig. 11. Result from LA-ICP-MS scanning (map2) on a pyrite crystal with inclusion-rich core and inclusion-absent domains (Sample 1506–187.84–188.08A). Note that the Co-rich areas correspond to smaller recrystallised pyrite crystals and inclusion-poor overgrowths. Arsenic is enriched in some parts in the core and within the overgrowths. The scale is in counts per second.

pyrite is a result of grain-scale zoning (Figs. 10 and 11). High relative As concentrations are also correlated locally with modestly increased Au concentrations (c. 0.1 ppm) as compared to other pyrites from Lovisa, which generally contain Au close to or below 0.01 ppm. The Co concentration is quite consistent around 5–50 ppm in all the major ore types, except in the late Sb-Ag-Cu-rich fracture fillings, in which the pyrite contains insignificant Co (<0.1 ppm; Fig. 8). Coarse-grained pyrite within calc-silicate assemblages locally overlying the Main Ore has the overall highest Co concentrations, reaching 2200 ppm, whereas lower Co concentrations were found in pyrite in adjacent veinlets. No clear differences were apparent between the inclusion-rich cores and inclusion-free overgrowths of the blastic pyrite crystals (Fig. 6C) in spot measurements, in part due to difficulties in analysing the former. Yet, a distinct zoning with respect to both As and Co was identified by LA-ICP-MS mapping of pyrite crystals from the Main Ore (Figs. 10 and 11). Cobalt is primarily enriched in the overgrowths (about one order of magnitude higher compared to the cores; Fig. 10), as well as in smaller, recrystallised pyrite crystals (Fig. 11). Arsenic can be higher both in core domains (Fig. 10) and in certain overgrowths (Fig. 11).

The only other trace element in pyrite that showed a systematic difference between ore types is Se. Similar to sphalerite, pyrite from the Sphalerite Ore is enriched in Se relative to pyrite from other ore types (Fig. 8). However, analytical spots of pyrite from the Sphalerite Ore are very limited.

Pyrite from the late Sb-Ag-Cu-rich fracture fillings in the Lovisa Fe Formation is anomalously enriched in Ag, Cd, Cu, In, Pb, Sb, Sn, Tl and Zn (Fig. 8). However, considering the few analytical spots, the small size of the pyrite and its occurrence as intergrowths with chalcopyrite (Fig. 7e-f), as well as the variable quality of the laser-ablation signals in this case, this trend needs to be viewed with some caution. However, the time-integrated analytical signal from the spot with the highest concentrations of these elements exhibits a stable plateau (ESM Fig. S3; Nr. 107) and the calculated concentrations are broadly consistent between different spots (Table 4). None of the very fine, euhedral pyrite crystals present as inclusions in the SFFs (Fig. 6f-h) were analysed.

4.3.4. *Chalcopyrite*

Besides Cu, Fe and S, only Ag, Au, Cd, Co, In, Sn, Tl and Zn were consistently detected in chalcopyrite from the Lovisa Fe Formation, whereas As, Bi, Ga, Ge, Hg, Mn, Mo, Pb, Sb, Se and Te abundances were more erratic (Tables 5 and ESM S4). Higher concentrations of the latter elements may reflect micro- to nanoscale inclusions of other minerals. The chalcopyrite trace element concentrations are very similar between the two textural types analysed, with only marginally higher Ag and Sb concentrations in the Sb-Ag-Cu-rich fracture fillings (Fig. 8). Chalcopyrite of both types contains detectable In (1 to 5 ppm) and Au concentrations (normally below 0.1 ppm).

4.3.5. *Pyrrhotite*

Pyrrhotite from the Lovisa Fe Formation is the main carrier of Co in these ores with concentrations of about 60 ppm. It also hosts Ni (35–55 ppm), As (110–150 ppm) and Mn (2–6 ppm; Tables 5 and ESM S4; Fig. 8). Pyrrhotite associated with pyrite alteration is locally enriched in Ag, As, Cd, Co, Cu, Ge, Mn, Ni, Pb, Sb and Tl.

4.3.6. *Tetrahedrite-group mineral*

The tetrahedrite-group mineral from the late Sb-Ag-Cu-rich sulphide-sulphosalt-fluorite fracture fillings in the Lovisa Fe Formation is the main carrier of Ag, Sb and Zn in these assemblages, but also contains Cd (1500–3200 ppm), Co (0.5–17 ppm), Ge (0.1–2 ppm), Sn (0.5–80 ppm) and Tl (0.5–16 ppm; Tables 5 and ESM S4). It also hosts detectable Au (0.1–7 ppm, and an outlier at 58 ppm); however, the laser-ablation signals show that Au is probably hosted by micro- to nanoscale inclusions of a Au-rich phase. Tentative formulae calculations based on

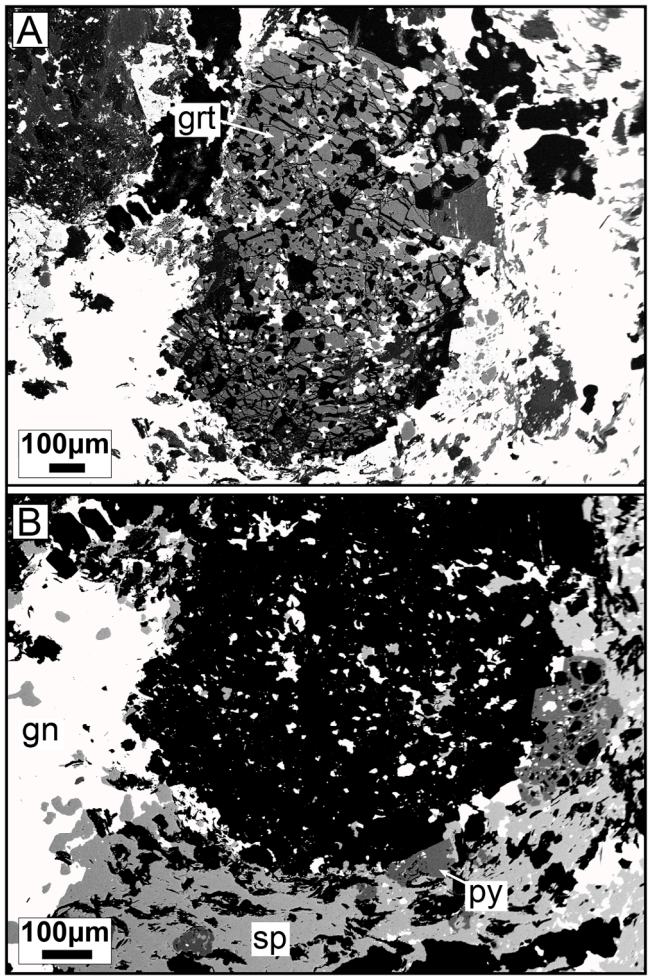

Fig. 12. Back-scattered images of highly fractured garnet clasts within a fine-grained and heavily deformed sulphide and silicate matrix. From a section of the Main Ore (sample 1506–187.84–188.08). Figures (A) and (B) represent the same garnet clast at different contrast and magnification. Abbreviations: gn – galena, grt – garnet, py – pyrite, sp – sphalerite.

cation concentrations ($\sum_{[Ag,Cu,Zn,Fe,Cd,Sb]} = 16$ apfu) from the LA-ICP-MS data show that the tetrahedrite-group mineral belongs to the freibergite series [$Ag_{6.05}(Cu_{4.2}Fe_{1.87}Cd_{0.04})Sb_{3.56}S_{13}$], corresponding to argentotetrahedrite-(Fe) (Table ESM 4; Biagioni et al., 2020).

5. Discussion

5.1. Mineral paragenesis and relative ore deformation and remobilisation

The Lovisa Zn-Pb deposit and the Lovisa Fe Formation are jointly interpreted as originally syngenetic exhalative deposits that formed in a vent-distal seafloor setting during periods of low volcanic activity at c. 1.89 Ga (Jansson et al., 2018). The Fe Formation formed before the Zn-Pb deposit and the two mineralising events were separated by a stage of explosive felsic volcanism and sedimentation. The Zn-Pb deposit most likely formed from saline and alkali-rich fluids, first depositing the stratiform Sphalerite Ore and subsequently the precursor to the sphalerite-galena Main Ore (Jansson et al., 2018).

Following primary ore formation, the ores and their host rocks were subjected to polyphase metamorphism and deformation during the Svecokarelian orogeny. The deformed character of the Lovisa Zn-Pb deposit was already recognised during exploration in the 1980s. Based on the observations of the prominent ball ore texture of the Main Ore and other meso- to microscopic structures and textures, the deformation and remobilisation of the ore were suggested to be polyphase (Carlon, 1987; Carlon and Bleeker, 1988). The main stage of ore deformation, including the development of the ball ore, was originally interpreted as synchronous with D_3 deformation (Carlon, 1987). In contrast, Jansson et al. (2018) recently proposed that the ball ore developed by deformation of an original galena-sphalerite layer late during the deformation phase associated with the development of the regional-scale Guldsmedshyttan syncline (here interpreted as D_2), while the SFFs were suggested to have formed either during later shearing or early in the transition to brittle conditions during the waning stages of the Svecokarelian orogeny.

The 3D tomography drill core scanning technique employed in this study revealed features related to deformation and remobilisation of the Lovisa ore that would be less informative or even overlooked during conventional drill core logging. By using these features in conjunction with other observations of meso- and microscale textures of the different ore types, we build upon previous work (Carlon, 1987; Carlon and Bleeker, 1988; Jansson et al., 2018) and present a refined interpretation of the sulphide ore paragenesis and relative timing of ore deformation and remobilisation in the Lovisa Zn-Pb deposit and the Lovisa Fe Formation.

During regional Svecokarelian metamorphism and deformation, the competence contrasts between the sulphide ore and the silicate-dominated host rocks, as well as the differences in primary depositional character and relative proportions of different ore minerals between the Main Ore (thicker bed with higher galena content) and the Sphalerite Ore (thinner laminae with low galena contents), would have greatly influenced the ore textures formed in and around the Lovisa ore body (e.g., Gilligan and Marshall, 1987; Marshall and Gilligan, 1987, 1993; Marshall et al., 2000; also noted in Jansson et al., 2018). Indeed, many of the observed textures, particularly the ball ore and Durchbewegung textures are readily explained by combinations of deformation and remobilisation of materials with contrasting properties. In these cases, remobilisation was mostly local (microscopic to metre-sized features) and probably dominated by fluid-assisted mechanical (solid-state) remobilisation (cf. Marshall et al., 2000). Deformation and remobilisation of the main sulphide assemblages thus probably commenced already during the broadly coeval D_1 and M_1 events. However, early ore textures indicative of deformation and remobilisation during this stage are difficult to recognise because of strong transposition of early structural features into D_2 fabrics, which is common for metamorphosed sulphide deposits (Klemd et al., 1987; Marshall and Gilligan, 1987). Yet, some early-formed garnet porphyroblasts/clasts, which are heavily deformed (Fig. 12), as well as minor, partly rounded pyrite porphyroblasts/clasts enclosed within a strongly deformed sulphide matrix in the Main Ore (Fig. 6a-b) may be remnants of the D_1-M_1 event. A generalised paragenetic table is shown in Fig. 13.

The conspicuous ball ore and Durchbewegung textures of the Main Ore are interpreted to have developed late during D_2 deformation associated with large-scale folding (Guldsmedshyttan syncline) and progressive, non-coaxial shearing within the high strain WBBZ. This is shown by angular to rounded clasts of gently folded host rock laminae within a strongly deformed and rotated sulphide matrix occurring in close vicinity to a D_2-related fold (Fig. 4a-b). This texture was probably accentuated during progressive deformation. The D_2 deformation phase was probably also responsible for producing many of the parasitic and smaller fold structures observed within the ore zones as well as the overall orebody geometry at Lovisa (Luth et al., 2019, 2022). Jansson et al. (2018) also noted parasitic folds in the Sphalerite Ore and suggested that this folding was related to layer-parallel shearing during D_2/D_3. Most of the macro and microscopic ore textures recognised, specifically of less competent sulphides infilling fractures in more competent minerals and rocks on different scales, are also inferred to have formed during the main D_2-(D_3)/M_2 phase and subsequent retrograde conditions (Fig. 13).

The SFFs are closely spatially linked with the remobilisation features.

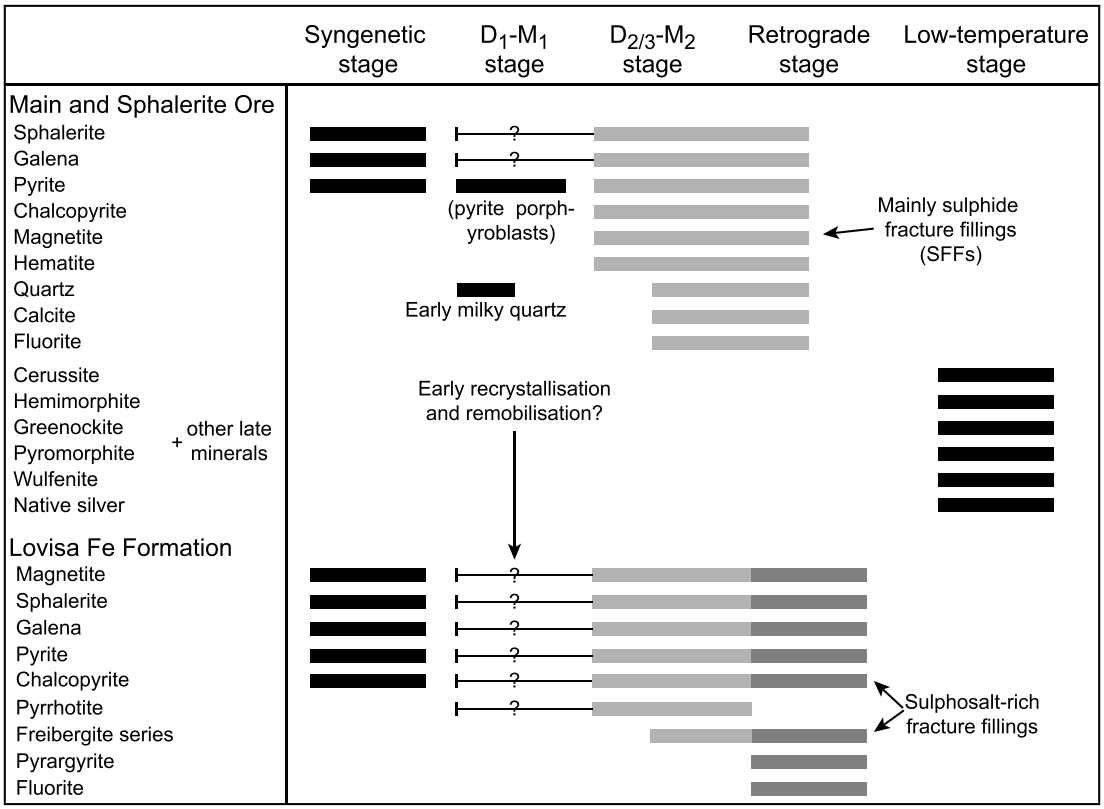

Fig. 13. A simplified paragenetic sequence for the Lovisa Zn-Pb ore and the Lovisa Fe Formation.

Many of the SFFs, if not all, were probably a result of mainly chemical (fluid-mediated) remobilisation of pre-existing sulphide ore (Marshall et al., 2000). The fact that most of the SFFs occur immediately adjacent to the two main ore zones, and less so above, between and below them, strongly supports this interpretation (cf. Gilligan and Marshall, 1987). For the SFFs, the scale of remobilisation is local, yet significantly larger (metres to tens of metres) than that characteristic of remobilisation features associated with dominantly solid-state mechanisms. The relative timing of formation of the SFFs is further constrained by: 1) SFFs crosscutting large garnet porphyroblasts (Fig. 6j), 2) galena-rich SSFs occurring in and propagating from fold hinges of small parasitic D_2 folds, 3) SFFs crosscutting $S_{0,1}$ layering and D_2-folded layers, 4) the presence of poorly developed ball ore textures in some of the SFFs, 5) calcite veinlets carrying minor sphalerite associated with post-D_2 micro faults (Fig. 4f-g) and 6) presence of locally extensive deformation twinning in calcite and sphalerite associated with the SFFs (Jonsson et al., 2020). The combined evidence corroborates the interpretation that the SFFs mainly formed during ductile–brittle and subsequent brittle conditions during D_2/D_3-M_2 and the subsequent retrograde stage (Fig. 13). A large proportion of the SFFs was probably associated with conspicuous, D_3-related and later NW-trending faults and fractures in the Lovisa area.

In the Lovisa Fe Formation, no mesoscale textures related to deformation are apparent from the 3D drill core scanning. Yet, abundant microscale textures indicate a strong metamorphic and tectonic overprint, with the sulphides mainly occurring as fracture fillings within, or as intergrowths with, metamorphic silicate assemblages and more competent ore minerals (Fig. 7a-d). Such features are commonly interpreted as formed during the transition to retrograde metamorphic conditions, e.g., as at Sulitjelma and other Zn-Cu deposits in the Norwegian Caledonides (Cook et al., 1993; Vokes and Craig, 1993). These sulphide-silicate-oxide textures at Lovisa can thus be most easily reconciled with a formation during the D_2/D_3-M_2 event and subsequent retrograde conditions (Fig. 13). The discordant and paragenetically late Sb-Ag-Cu-rich sulphide-sulphosalt-fluorite fracture infillings, however, show no clear signs of deformation. In the Hällefors district, located about 40 km W-NW of Lovisa, in part similar Ag-rich sulphide-sulphosalt veins and fracture fillings were demonstrated to have formed via metamorphic remobilisation at around 300–400 °C and 200–300 MPa (Wagner et al., 2005). The lack of visible features of deformation suggests that the Sb-Ag-Cu-rich fracture fillings at Lovisa formed during late retrograde conditions by metamorphic remobilisation (Fig. 13).

The latest phase of ore modification and local overprinting leading to new mineral formation is manifested by characteristic low-temperature minerals such as cerussite, hemimorphite, greenockite, pyromorphite, wulfenite, native silver and others occurring in late fractures and corrosion pockets in the ore zones at Lovisa (Fig. 13; e.g., Nysten and Lorin, 2021).

5.2. *Trace element (re-)distribution trends*

Based on the results of the trace element analysis and observations of the general abundances of different ore minerals in the Lovisa Zn-Pb deposit, sphalerite is the main carrier of Cd, Co, Ge, Hg and In, galena is the primary host for Ag, Bi, Sb, Se, Te, and Tl, and pyrite is the principal carrier of Au, As, Mo and Ni, and in certain domains also Co. Gallium concentrations are overall low in the sulphides and below 1 ppm in sphalerite, i.e., comparable to many other polymetallic sulphide deposits in Bergslagen (Cook et al., 2009; Jonsson and Högdahl, 2019). Rather, Ga is hosted by silicates in the ore (as indicated from LA-ICP-MS mapping; Fig. 11). In the Lovisa Fe Formation, in which pyrrhotite and chalcopyrite are part of the ore assemblages, pyrrhotite is the primary host for Co and Ni and in part As (ESM Fig. S4). Chalcopyrite is seldom the main carrier of any trace element, apart from In when sphalerite is rare, as in the Sb-Ag-Cu-rich sulphide-sulphosalt-fluorite fracture infillings (Fig. 8). The trace element partitioning between sulphides at Lovisa is in line with results from previous studies of primary and metamorphosed hydrothermal sulphide deposits globally (George et al., 2016; Zhao et al., 2021).

The concentrations of trace elements in the Lovisa Zn-Pb deposit are overall lower than in other studied sulphide deposits in Bergslagen (Cook et al., 2009; George et al., 2016; Kampmann et al., 2018; Tiu et al., 2021). In comparison to the major stratiform ash-siltstone-hosted (SAS) type sulphide deposit (Zinkgruvan), the sphalerite from Lovisa is notable for carrying higher In concentrations (up to 20 ppm compared to < 0.5 ppm), but lower Co (up to 30 ppm compared to $\sim$ 90 to 490 ppm), whereas other trace elements are comparable (Axelsson and Rodushkin, 2001; Cook et al., 2009).

The different SFFs exhibit partly different trace element signatures and mineralogy (Figs. 8 and 9), which can be correlated with their local environments. Sphalerite-rich SFFs hosted within the Sphalerite Ore show similar trace element trends as the sphalerite from this ore (Figs. 8 and 9), while the galena-sphalerite SFFs adjacent to the Main Ore, in turn, have sphalerite trace element compositions akin to sphalerites from that ore. The higher galena content of these SFFs is consistent with galena being more abundant in the Main Ore and more easily remobilised than sphalerite. Moreover, sphalerite and galena from the breccia contact of the Main Ore show similar trace element signatures and textures as the SSFs. This indicates that the peripheral, breccia-like domains of the Main Ore are largely gradational to the SFFs and increasingly composed of remobilised material, yet they retained their "Main Ore" trace element signature. The above observations suggest a dominant control by local host rock and ore domains on the sulphide mineralogy and trace element compositions of the different sulphides in the remobilised SFFs. Because the mineralogy of the SSFs is controlled by the local environment, the SSFs could not be classified based on both orientation and mineralogy, even though the presence of local cross-cutting relationships indicate different generations of SSFs. In general, only minor redistribution of trace elements occurred during metamorphism and remobilisation in the Lovisa Zn-Pb deposit. Possible exceptions from this are Bi and Se, which are locally anomalously enriched in some galena-rich SFFs, and Co, as shown by Co-enriched, late growth domains of pyrite crystals (Figs. 10 and 11). This internal redistribution of Co, which tentatively also is inferred by the very Co-rich, coarse pyrite locally found above the Main Ore (Fig. 8), is suggested to be a late metamorphic feature that occurred during the D_2/D_3-M_2 stages.

In the Lovisa Fe Formation, the presence of the late Sb-Ag-Cu-rich sulphide-sulphosalt-fluorite fracture infillings suggest a greater redistribution of trace elements as compared to the Lovisa Zn-Pb deposit. In addition, the sulphides in the earliest assemblages of the Lovisa Fe Formation are more enriched in the same suite of elements as found in the sulphide-sulphosalt-fluorite fracture infillings (mainly Ag, Cu, Pb and Sb), as compared to the sulphides in the Lovisa Zn-Pb deposit. The primary metal inventory and concentrations in sulphides are thus suggested to be the major controls on the extent of trace element redistribution and formation of new minerals during the metamorphic remobilisation events. This is further indicated by the greater trace element redistribution and new mineral formation during metamorphic remobilisation in the Lappberget Zn-Pb-Ag-(Cu-Au) deposit (Tiu et al., 2021) and the Falun Zn-Pb-Cu-(Au-Ag) deposit (Kampmann et al., 2018) in Bergslagen as well as in the Ge-rich Zn-Pb deposits in the Pyrenean Axial Zone (Cugerone et al., 2020), all in which the primary sulphides generally hosted higher concentrations of a significantly more diverse suite of trace elements than at Lovisa.

5.3. Comparisons with other deformed and metamorphosed deposits

The Lovisa Zn-Pb deposit and underlying Fe Formation share several features with other deformed and metamorphosed stratiform sulphide-rich deposits. Two key examples are the Zn-Pb deposits in the Cinco Villas Massif, Spain (Pesquera and Velasco, 1993) and the Cu-(Zn) Matchless deposit, Namibia (Klemd et al., 1987; Cook et al., 1994). Both occurrences experienced a protracted, polyphase (D_1 to D_3) deformation history with associated amphibolite facies metamorphism. In the Matchless deposit, banded ore gradually grades into thicker, more massive-type ore exhibiting well-developed Durchbewegung textures with angular to rounded host rock fragments within a chalcopyrite-pyrrhotite-rich ductile matrix (Klemd et al., 1987; Cook et al., 1994). Piercement structures have developed along the contacts of the ore with the host rock and have disrupted small-scale folds (comparable with Fig. 4a; Klemd et al., 1987). In the Cinco Villas Massif, similar Durchbewegung and piercement textures and structures have developed within banded to massive-type, deformed sulphide ores with sphalerite, galena, pyrrhotite and pyrite (Pesquera and Velasco, 1993).

At both localities, different generations of sulphide + quartz ± carbonate ± fluorite ± barite fracture fillings and veins are also present. In the Cinco Villas Massif, the volumetrically most important veins formed after the deformation stages associated with folding and the generation of major foliation (D_2), and consist of the same sulphide assemblages as in the banded and massive ores (Pesquera and Velasco, 1993). In the Matchless deposit, coarse-grained chalcopyrite-pyrrhotite veins formed mostly during the late deformation stages (D_2 and D_3, Klemd et al., 1987). Similar to the SFFs in the Lovisa Zn-Pb deposit, the veins and fracture fillings from these two examples display deformation features (such as deformation twinning, "micro ball ores" textures and minor brecciation) that indicate that they formed by localised remobilisation during ductile–brittle and subsequent brittle conditions and that the sulphide mineralogy is controlled by the composition of the precursor ores (Klemd et al., 1987; Pesquera and Velasco, 1993; Cook et al., 1994).

Another feature that is shared by many other metamorphosed sulphide deposits is the occurrence of mainly late sulphosalt-bearing veins, fracture fillings and mineral assemblages similar to those found in the Lovisa Fe Formation, e.g., as in the Bleikvassli Zn-Pb-(Cu) deposit, Norway (Cook et al., 1998), the Barika deposit, Iran (Tajeddin et al., 2019) and the Rampura-Agucha Zn-Pb-(Ag) deposit, India (Höller and Gandhi, 1995; Mishra and Bernhardt, 2009). While most commonly explained by fluid-mediated (chemical) remobilisation during late metamorphic conditions, some of these features have been attributed to the remobilisation of sulphide melts (cf. Frost et al., 2002; Mishra and Bernhardt, 2009). In light of the occurrence of Sb-Ag-Cu-rich sulphide-sulphosalt-fluorite fracture fillings in the Lovisa Fe Formation, an assessment may be warranted regarding the potential role of sulphide anatexis in remobilisation as such melts can be highly mobile during deformation (Frost et al., 2002; Tomkins et al., 2006, 2007). Indeed, variable degrees of ore remobilisation by sulphide melt formation have been proposed to have taken place during metamorphism of massive Pb-Zn ± Cu deposits at different metamorphic conditions, ranging from chiefly amphibolite to granulite but locally also greenschist facies, with examples including the Sindesar Khurd Pb-Zn-Ag deposit, India (Pruseth et al., 2016), the Balmat Zn deposit, USA (Matt et al., 2019), the Montauban Zn-Pb-Au-Ag deposit, Canada (Tomkins et al., 2007) and the Broken Hill Zn-Pb-Ag deposit, Australia (Frost et al., 2002; Tomkins et al., 2007; Spry et al., 2008). Common to such deposits is that they contain significant proportions of either sulphosalts containing low-melting point chalcophile elements (e.g., Ag, As, Bi, Sb, Se and Te) concentrated in discrete veins and pockets (Frost et al., 2002), or arsenopyrite-dominated assemblages (Tomkins et al., 2006).

In the Lovisa Zn-Pb deposit, which exhibits a mineralogy dominated by sphalerite-galena and subordinate pyrite and negligible arsenopyrite and sulphosalts, remobilisation by sulphide anatexis is deemed unlikely. Textural evidence supporting it is also lacking. However, the Lovisa Fe Formation would be more prone to such a process because the sulphide mineralogy is more diverse and sulphosalts are present. Yet, aside from the discrete Sb-Ag-Cu-rich sulphide-sulphosalt-fluorite fracture fillings, no textural evidence directly supporting ore remobilisation by sulphide anatexis, such as the occurrence of multiphase sulphide and sulphosalts inclusions representing originally homogeneous melt droplets (e.g., Frost et al., 2002; Matt et al., 2019) have been observed. Because the sulphosalt-bearing fracture fillings can be temporally linked to the late retrograde metamorphic stage when the conditions likely was too cold for melting, our preferred interpretation is formation by dominantly fluid-mediated (chemical) remobilisation.

5.4. Genetic links to the nearby Cu-Co deposits

The sulphides in the SAS-type Lovisa Zn-Pb deposit and Fe Formation host Co concentrations that are lower than at the comparable Zinkgruvan deposit, but generally higher than the sulphides from SVALS-type deposits in Bergslagen (Kampmann et al., 2018, Tiu et al., 2021). The difference can likely be explained by the higher capability of Co transport in the oxidised ore-forming fluids inferred for SAS-type deposits compared to the reducing fluids that formed SVALS-type deposits in Bergslagen (Jansson and Liu, 2020). The presence of Co in the sulphides potentially points to a genetic link with the nearby Cu-Co deposits, including the previously mined Håkansboda Cu-Co deposit ~ 1.5 km NE of Lovisa (Figs. 2 and 3; Carlon and Bleeker, 1988; Jansson et al., 2018). Such a relationship has been proposed for Zinkgruvan, where Cu-Co-rich stratabound, carbonate-hosted mineralisation occurs in the stratigraphic footwall to the stratiform Zn-Pb-Ag deposit (Hedstroem et al., 1989; Jansson et al., 2017). At Zinkgruvan, oxidised, metal-bearing saline hydrothermal fluids with near-neutral pH interacted with organic matter and mixed with reduced pore waters to form the Cu-Co mineralisation in a vent-proximal, subseafloor setting. The Zn-Pb-Ag deposit, in turn, formed in a vent-distal setting following the exhalation of the oxidised fluids into a reducing seafloor environment (Jansson et al., 2017; Jansson and Liu, 2020; Stephens and Jansson, 2020). The genetic link between these two mineralisation styles was in part based on the overall Co-rich character of sphalerite as well as the gradually increasing Zn/Pb of the ores and the decreasing sphalerite Co concentrations from proximal to distal within the Zn-Pb-Ag deposit (Jansson et al., 2017; Jansson and Liu, 2020).

The origin of the Håkansboda Cu-Co mineralisation has been attributed to vent-proximal replacement of carbonate host rocks by Cu-Co sulphides with contemporaneous formation of exhalative Zn-Pb and Fe oxide mineralisation at Lovisa in a vent-distal setting (Carlon and Bleeker, 1988; Jansson and Liu, 2020). This inferred distal nature can explain the Co-poor character of the mineralisation at Lovisa, analogous to the most distal portions of the Zinkgruvan ore zone (Jansson and Liu, 2020). Furthermore, the Cu-Co deposits in the Lovisa area occur in the stratigraphic footwall of the Zn-Pb mineralisation, which is similar to Zinkgruvan. Regarding metal zonation in the Lovisa Zn-Pb sulphide ore, the gradual disappearance of the Sphalerite Ore towards the northern part of the deposit results in an apparent Pb/Zn zonation of the bulk ore (Pb/Zn decreases towards the south; Jansson et al., 2018). However, more detailed studies of the metal zonation within individual ore zones are needed as the Main Ore and Sphalerite Ore are likely to have formed at different times by different fluid pulses (Jansson et al., 2018). Yet, a Pb/Zn zonation has tentatively been recognised in the Main Ore based on data from its successive mining and shows decreasing Pb:Zn ratios from the upper central parts of this ore downwards and to the south.

The structurally complex nature of the Håkansboda Cu-Co deposit, where at least two phases of folding affected the ore, strongly implies that it formed prior to Svecokarelian polyphase deformation and regional metamorphism (Carlon and Bleeker, 1988). This led to the development of ball ore textures in massive sulphide ores with the wall rock contacts brecciated and filled with sulphide veins cross-cutting the tectonic foliation. It also led to significant recrystallisation of ore assemblages and other features indicating deformation and remobilisation of primary sulphide ores during D_3 (Carlon and Bleeker, 1988). These features overall suggest that the Cu-Co and Zn-Pb mineralisation types in the Lovisa-Håkansboda area have a shared deformation history, albeit with slight local differences, and are permissive for a genetic link between the two.

6. Conclusions

This study reinforces the interpretation that the Lovisa Zn-Pb deposit and the underlying Fe Formation represent metamorphosed and locally strongly deformed syngenetic exhalative deposits. The Lovisa Zn-Pb deposit comprises a common sulphide paragenesis dominated by sphalerite and galena with subordinate pyrite. Based on the textural features recognised in this study, deformation of the primary ore commenced during the first stage of regional metamorphism and deformation (D_1-M_1; 1.87–1.85 Ga), although most early textures were obliterated and transposed to D_2-related features. The main deformation of the sulphide ore occurred during the second stage of regional deformation and metamorphism synchronous with regional-scale folding (D_2-M_2; c. 1.83–1.80 Ga). This caused the development of the distinct ball ore features and Durchbewegung textures of the sphalerite-galena massive ore and metamorphosed laminated textures in sphalerite-rich ores. Significant remobilisation of primary sulphides led to the formation of abundant sphalerite-galena fracture fillings close to the main ore horizons and chemically and mineralogically contrasting sulphide-sulphosalt-fluorite fracture fillings in the Lovisa Fe Formation. The formation of the various fracture fillings extended through late retrograde and brittle conditions.

Trace element deportment between sulphides is in line with many other exhalative sulphide deposits worldwide. The sulphide ore at the Lovisa Zn-Pb deposit generally hosts low concentrations of trace elements and exhibits a simple mineralogy, as compared to the more complex sulphide ore in the Lovisa Fe Formation. The mineralogy and trace element signatures of remobilised sulphide fracture infillings were primarily controlled by the character of the local ore domains from which the components originated. Variable, but generally minor redistribution of trace elements occurred during remobilisation. A notable exception to this is Co, which was locally enriched in pyrite overgrowths and late recrystallised pyrite.

The utilisation of the concurrent XCT and XRF scanning technique has improved the capacity for interpretations of ore textures by adding a third dimension to micro- to macroscale observations and data yielded by traditional methods. The present applications to the Lovisa deposit show that it not only offers improvements for practical implementation in exploration and mining, but also for more fundamental research issues such as textural and structural studies of ore deposits and their evolution and modification over time.

Declaration of Competing Interest

The authors declare that they have no known competing financial interests or personal relationships that could have appeared to influence the work reported in this paper.

Acknowledgements

This study is part of the X-MINE project funded by the European Union's Horizon 2020 research and innovation program under grant agreement 730270. The staff at Lovisagruvan working within the X-MINE project is greatly acknowledged, as are students involved in the project at Uppsala University. We thank Jarek Majka (Uppsala University) for assistance with the FE-EPMA analysis, and Matthias Konrad-Schmolke (University of Gothenburg) for discussions regarding LA-ICP-MS/MS mapping. Constructive comments from Nils Jansson, Paul G. Spry and two anonymous reviewers on different versions of this manuscript are greatly acknowledged.

Appendix A. Supplementary data

Supplementary data to this article can be found online at https://doi.org/10.1016/j.oregeorev.2021.104611.

References

Allen, R.L., Lundström, I., Ripa, M., Simeonov, A., Christofferson, H., 1996. Facies analysis of a 1.9 Ga, continental margin, back-arc, felsic caldera province with diverse Zn-Pb-Ag-(Cu-Au) sulfide and Fe oxide deposits, Bergslagen Region. Sweden. Econ. Geol. 91, 979–1006. https://doi.org/10.2113/gsecongeo.91.6.979.

Andersson, U.B., Högdahl, K., Sjöstrom, H., Bergman, S., 2006. Multistage growth and reworking of the Palaeoproterozoic crust in the Bergslagen area, southern Sweden: evidence from U-Pb geochronology. Geol. Mag. 143, 679–697. https://doi.org/10.1017/S0016756806002494.

Andersson, S.S., Jonsson, E., Högdahl, K., 2016. Metamorphism and deformation of a Palaeoproterozoic polymetallic sulphide – oxide mineralisation: Hornkullen, Bergslagen, Sweden. GFF 138, 410–423. https://doi.org/10.1080/11035897.2015.1135187.

Axelsson, M.D., Rodushkin, I., 2001. Determination of major and trace elements in sphalerite using laser ablation double focusing sector field ICP-MS. J. Geochemical Explor. 72, 81–89. https://doi.org/10.1016/S0375-6742(00)00166-7.

Bergqvist, M., Landström, E., Landström, E., Luth, S., 2019. Access to geological structures, density, minerals and textures through novel combination of 3D tomography, XRF and sample weight. ASEG. Ext. Abstr. 2019, 1–3. https://doi.org/10.1080/22020586.2019.12073146.

Beunk, F.F., Kuipers, G., 2012. The Bergslagen ore province, Sweden: Review and update of an accreted orocline, 1.9-1.8 Ga BP. Precambr. Res. 216–219, 95–119. https://doi.org/10.1016/j.precamres.2012.05.007.

Biagioni, C., George, L.L., Cook, N.J., Makovicky, E., Moëlo, Y., Pasero, M., Sejkora, J., Stanley, C.J., Welch, M.D., Bosi, F., 2020. The tetrahedrite group: Nomenclature and classification. Am. Mineral. 105, 109–122. https://doi.org/10.2138/am-2020-7128.

Carlon, C.J., 1987. The Lovisa project 1985–1986. Unpublished exploration report for Luossavaara-Kirunavaara Aktiebolag (LKAB) and British Petroleum (BP) AB Joint Venture B87-1, p. 127.

Carlon, C.J., Bleeker, W., 1988. The geology and structural setting of the Håkansboda Cu-Co-As-Sb-Bi-Au deposit and associated Pb-Zn-Cu-Ag-Sb mineralisation, Bergslagen, central Sweden. Geol. Mijnbouw 67, 272–292.

Cioacă, M.-E., Munteanu, M., Lynch, E.P., Arvanitidis, N., Bergqvist, M., Costin, G., Ivanov, D., Milu, V., Arvidsson, R., Iorga-pavel, A., Högdahl, K., Stoilov, V., 2020. Mineralogical setting of precious metals at the Assarel Porphyry copper-gold Deposit, Bulgaria, as supporting information for the development of new drill Core 3D XCT-XRF scanning technology. Minerals 10, 946. https://doi.org/10.3390/min10110946.

Cook, N.J., Halls, C., Boyle, A.P., 1993. Deformation and metamorphism of massive sulphides at Sulitjelma. Norway. Mineral. Mag. 57, 67–81. https://doi.org/10.1180/minmag.1993.057.386.07.

Cook, N.J., Klemd, R., Okrusch, M., 1994. Sulphide mineralogy, metamorphism and deformation in the Matchless massive sulphide deposit. Namibia. Miner. Depos. 1–15. https://doi.org/10.1007/BF03326392.

Cook, N.J., Spry, P.G., Vokes, F.M., 1998. Mineralogy and textural relationships among sulphosalts and related minerals in the Bleikvassli Zn-Pb-(Cu) deposit, Nordland. Norway. Miner. Depos. 34, 35–56. https://doi.org/10.1007/s001260050184.

Cook, N.J., Ciobanu, C.L., Pring, A., Skinner, W., Shimizu, M., Danyushevsky, L., Saini-Eidukat, B., Melcher, F., 2009. Trace and minor elements in sphalerite: A LA-ICPMS study. Geochim. Cosmochim. Acta 73, 4761–4791. https://doi.org/10.1016/j.gca.2009.05.045.

Cugerone, A., Cenki-Tok, B., Muñoz, M., Kouzmanov, K., Oliot, E., Motto-Ros, V., Le Goff, E., 2021. Behavior of critical metals in metamorphosed Pb-Zn ore deposits: Example from the Pyrenean Axial Zone. Miner. Depos. 56, 685–705. https://doi.org/10.1007/s00126-020-01000-9.

Danyushevsky, L., Robinson, P., Gilbert, S., Norman, M., Large, R., McGoldrick, P., Shelley, M., 2011. Routine quantitative multi-element analysis of sulphide minerals by laser ablation ICP-MS: Standard development and consideration of matrix effects. Geochemistry Explor. Environ. Anal. 11, 51–60. https://doi.org/10.1144/1467-7873/09-244.

Frost, B.R., Mavrogenes, J.A., Tomkins, A.G., 2002. Partial melting of sulphide ore deposits during medium- and high-grade metamorphism. Can. Mineral. 40, 1–18. https://doi.org/10.2113/gscanmin.40.1.1.

Fougerouse, D., Micklethwaite, S., Tomkins, A.G., Mei, Y., Kilburn, M., Guagliardo, P., Fisher, L.A., Halfpenny, A., Gee, M., Paterson, D., Howard, D.L., 2016. Gold remobilisation and formation of high grade ore shoots driven by dissolution-reprecipitation replacement and Ni substitution into auriferous arsenopyrite. Geochim. Cosmochim. Acta 178, 143–159. https://doi.org/10.1016/j.gca.2016.01.040.

Gaál, G., Gorbatschev, R., 1987. An Outline of the Precambrian Evolution of the Baltic Shield. Precambrian Res. 35, 15–52. https://doi.org/10.1016/0301-9268(87)90044-1.

Geijer, P., 1971. Sulfidic "ball ores" and the pebble dykes. Geological Survey of Sweden C 662, 1–29.

Geijer, P., Magnusson, N.H., 1944. De mellansvenska järnmalmernas geologi. Geological Survey of Sweden Ca 35, 654 pp.

George, L.L., Cook, N.J., Ciobanu, C.L., 2016. Partitioning of trace elements in co-crystallized sphalerite-galena-chalcopyrite hydrothermal ores. Ore Geol. Rev. 77, 97–116. https://doi.org/10.1016/j.oregeorev.2016.02.009.

Gilbert, S.E., Danyushevsky, L.V., Goemann, K., Death, D., 2014. Fractionation of sulphur relative to iron during laser ablation-ICP-MS analyses of sulphide minerals: Implications for quantification. J. Anal. At. Spectrom. 29, 1024–1033. https://doi.org/10.1039/C4JA00012A.

Gilligan, L.B., Marshall, B., 1987. Textural evidence for remobilization in metamorphic environments. Ore Geol. Rev. 2, 205–229. https://doi.org/10.1016/0169-1368(87)90029-1.

Griffin, L.W., Power, W.J., Pearson, N.J., ÓReilly, S.Y., 2008. GLITTER: Data reduction software for laser ablation ICP-MS. In: Sylvester, P. (Ed.), Laser Ablation ICP-MS in the Earth Sciences: Current Practices and Outstanding Issues. Mineralogical Association of Canada, pp. 308–311.

Hedstroem, P., Simeonov, A., Malmstrom, L., 1989. The Zinkgruvan ore deposit, south-central Sweden; a Proterozoic, proximal Zn-Pb-Ag deposit in distal volcanic facies. Econ. Geol. 84, 1235–1261. https://doi.org/10.2113/gsecongeo.84.5.1235.

Hermansson, T., Stephens, M.B., Corfu, F., Page, L.M., Andersson, J., 2008. Migratory tectonic switching, western Svecofennian orogen, central Sweden: Constraints from U/Pb zircon and titanite geochronology. Precambr. Res. 161, 250–278. https://doi.org/10.1016/j.precamres.2007.08.008.

Hogmalm, K.J., Zack, T., Karlsson, A.-O., Sjöqvist, A.S.L., Garbe-Schönberg, D., 2017. In situ Rb-Sr and K-Ca dating by LA-ICP-MS/MS: An evaluation of N2O and SF6 as reaction gases. J. Anal. At. Spectrom. 32, 305–313. https://doi.org/10.1039/C6JA00362A.

Höller, W., Gandhi, S.M., 1995. Silver-bearing sulfosalts from the metamorphosed Rampura Agucha Zn-Pb-(Ag) deposit, Rajasthan. India. Can. Mineral. 33, 1047–1057.

Jansson, N.F., Allen, R.L., 2015. Multistage ore formation at the Ryllshyttan marble and skarn-hosted Zn-Pb-Ag-(Cu)+magnetite deposit, Bergslagen. Sweden. Ore Geol. Rev. 69, 217–242. https://doi.org/10.1016/j.oregeorev.2015.02.018.

Jansson, N.F., Zetterqvist, A., Allen, R.L., Billström, K., Malmström, L., 2017. Genesis of the Zinkgruvan stratiform Zn-Pb-Ag deposit and associated dolomite-hosted Cu ore, Bergslagen. Sweden. Ore Geol. Rev. 82, 285–308. https://doi.org/10.1016/j.oregeorev.2016.12.004.

Jansson, N.F., Sädbom, S., Allen, R.L., Billström, K., Spry, P.G., 2018. The Lovisa Stratiform Zn-Pb deposit, Bergslagen, Sweden: Structure, stratigraphy, and ore genesis. Econ. Geol. 113, 699–739. https://doi.org/10.5382/econgeo.2018.4567.

Jansson, N.F., Liu, W., Jansson, N.F., 2020. Controls on cobalt and nickel distribution in hydrothermal sulphide deposits in Bergslagen, Sweden - constraints from solubility modelling. GFF 142, 87–95. https://doi.org/10.1080/11035897.2020.1751270.

Jochum, K.P., Weis, U., Stoll, B., Kuzmin, D., Yang, Q., Raczek, I., Jacob, D.E., Stracke, A., Birbaum, K., Frick, D.A., Günther, D., Enzweiler, J., 2011. Determination of reference values for NIST SRM 610–617 glasses following ISO guidelines. Geostand. Geoanalytical Res. 35, 397–429. https://doi.org/10.1111/j.1751-908X.2011.00120.x.

Johansson, Å., Stephens, M.B., 2017. Timing of magmatism and migmatization in the 2.0–1.8 Ga accretionary Svecokarelian orogen, south-central Sweden. Int. J. Earth Sci. 106, 783–810. https://doi.org/10.1007/s00531-016-1359-3.

Jonsson, E., 2004. Fissure-Hosted Mineral Formation and Metallogenesis in the Långban Fe–Mn–(Ba–As–Pb–Sb...) Deposit, Bergslagen, Sweden. Stockholm University, Sweden, p. 110.

Jonsson, E., Högdahl, K., 2019. On the occurrence of gallium and germanium in the Bergslagen ore province, Sweden. GFF 141, 48–53. https://doi.org/10.1080/11035897.2018.1525619.

Jonsson, E., Andersson, S.S., Sahlström, F., Högdahl, K., 2020. Sphalerite deformation highlighted by chemical etching with reflected polarised light darkfield and differential interference contrast microscopy. 34th Nordic Geological Winter Meeting, Oslo.

Kampmann, T.C., Jansson, N.F., Stephens, M.B., Olin, P.H., Gilbert, S., Wanhainen, C., 2018. Syn-tectonic sulphide remobilization and trace element redistribution at the Falun pyritic Zn-Pb-Cu-(Au-Ag) sulphide deposit, Bergslagen. Sweden. Ore Geol. Rev. 96, 48–71. https://doi.org/10.1016/j.oregeorev.2018.04.010.

Ketcham, R.A., Carlson, W.D., 2001. Acquisition, optimization and interpretation of x-ray computed tomographic imagery: Applications to the geosciences. Comput. Geosci. 27, 381–400. https://doi.org/10.1016/S0098-3004(00)00116-3.

Klemd, R., Maiden, K.J., Okrusch, M., 1987. The Matchless copper deposit, South West Africa/Namibia: A deformed and metamorphosed massive sulfide deposit. Econ. Geol. 82, 587–599. https://doi.org/10.2113/gsecongeo.82.3.587.

Kyle, J.R., Ketcham, R.A., 2015. Application of high resolution X-ray computed tomography to mineral deposit origin, evaluation, and processing. Ore Geol. Rev. 65, 821–839. https://doi.org/10.1016/j.oregeorev.2014.09.034.

König, S., Eickmann, B., Zack, T., Yierpan, A., Wille, M., Taubald, H., Schoenberg, R., 2019. Redox induced sulfur-selenium isotope decoupling recorded in pyrite. Geochim. Cosmochim. Acta 244, 24–39. https://doi.org/10.1016/j.gca.2018.09.013.

Lockington, J.A., Cook, N.J., Ciobanu, C.L., 2014. Trace and minor elements in sphalerite from metamorphosed sulphide deposits. Mineral. Petrol. 108, 873–890. https://doi.org/10.1007/s00710-014-0346-2.

Lovisagruvan AB, 2020. Annual report 2019. www.lovisagruvan.se.

Lundström, I., 1983. Beskrivning till Berggrundskartan. Lindesberg SV. Geological Survey of Sweden Af 126, 140 pp.

Luth, S., Sahlström, F., Jansson. N., Jönberger, J., Sädbom, S., Landström, E., Bergqvist, M., Arvanitidis, N., Arvidsson, R., 2019. Building 3D geomodels using XRF-XRT-generated drill core data: The Lovisa-Håkansboda base metal-and Stråssa-Blanka iron deposits in Bergslagen, Sweden. Proceedings 15th SGA Biennial Meeting 2019, Glasgow, Scotland 3, 1282–1285.

Luth, S., Bergman, S., 2020. Regional strukturanalys i Bergslagen – från lineament till skjuvzon. Geological Survey of Sweden 2020:13, p. 37.

Luth, S., Sahlström, F., Bergqvist, M., Hansson, A., Lynch, E.P., Sädbom, S., Jonsson, E., Andersson, S.S., Arvanitidis, N., 2022. Combined XCT-XRF drill core scanning for 3D rock and ore characterization: Implications for the Lovisa stratiform Zn-Pb deposit and its structural setting, Bergslagen, Sweden. Econ. Geol. In press.

Marshall, B., Gilligan, L.B., 1987. An introduction to remobilization: Information from ore-body geometry and experimental considerations. Ore Geol. Rev. 2, 87–131. https://doi.org/10.1016/0169-1368(87)90025-4.

Marshall, B., Gilligan, L.B., 1989. Durchbewegung structure, piercement cups, and piercement veins in massive sulfide deposits: Formation and interpretation. Econ. Geol. 84, 2311–2319. https://doi.org/10.2113/gsecongeo.84.8.2311.

Marshall, B., Gilligan, L.B., 1993. Remobilization, syn-tectonic processes and massive sulphide deposits. Ore Geol. Rev. 8, 39–64. https://doi.org/10.1016/0169-1368(93)90027-V.

Marshall, B., Vokes, F.M., Larocque, A.C.I., 2000. Regional metamorphic remobilization: upgrading and formation of ore deposits. Rev. Econ. Geol. 11, 19–38.

Matt, P., Power, W., deLorraine, W.F., Chiarenzelli, J., 2019. Sulfide and silicate anatexis in the Balmat zinc deposit (New York, USA) and its implications for ore remobilization. Ore Geol. Rev. 107, 392–401. https://doi.org/10.1016/j.oregeorev.2019.03.002.

Mishra, B., Bernhardt, H.-J., 2009. Metamorphism, graphite crystallinity, and sulfide anatexis of the Rampura-Agucha massive sulfide deposit, northwestern India. Miner. Depos. 44, 183–204. https://doi.org/10.1007/s00126-008-0208-0.

Munteanu, M., Sädbom, S., Paaso, J., Bergqvist, M., Arvanitidis, N., Arvidsson, R., Kolacz, J., Bakalis, E., Ivanov, D., Grammi, K., Kalliopuska, J., Polansky, S., Gielda, M., Björklund, J.-E., Sartz, L., Högdahl, K., Attiwell, P., Lynch, E., Luth, S., Bakker, E., 2020. X-MINE project (H2020): testing the capabilities of X-ray techniques in drill core scanning and ore sorting. EGU General Assembly Conference Abstracts. p. 11216.

Nysten, P., Lorin, T., 2021. Lovisagruvan – ett mineralogiskt eldorado i det lilla formatet. Geologiskt Forum 109, 4–11.

Onuk, P., Melcher, F., Mertz-Kraus, R., Gäbler, H.-E., Goldmann, S., 2017. Development of a matrix-matched sphalerite reference material (MUL-ZnS-1) for calibration of in situ trace element measurements by laser ablation-inductively coupled plasma-mass spectrometry. Geostand. Geoanalytical Res. 41, 263–272. https://doi.org/10.1111/ggr.2017.41.issue-210.1111/ggr.12154.

Paton, C., Hellstrom, J., Paul, B., Woodhead, J., Hergt, J., 2011. Iolite: Freeware for the visualisation and processing of mass spectrometric data. J. Anal. At. Spectrom. 26, 2508–2518. https://doi.org/10.1039/c1ja10172b.

Pesquera, A., Velasco, F., 1993. Ore metamorphism in sulfide mineralizations from the Cinco Villas Massif (Western Pyrenees, Spain). Econ. Geol. 88, 266–282. https://doi.org/10.2113/gsecongeo.88.2.266.

Pruseth, K.L., Mishra, B., Jehan, N., Kumar, B., 2016. Evidence of sulfide melting and melt fractionation during amphibolite facies metamorphism of the Rajpura-Dariba polymetallic sulfide ores. Ore Geol. Rev. 72, 1213–1223. https://doi.org/10.1016/j.oregeorev.2015.03.012.

Ramdohr, P., 1955. Die Erzmineralien und ihre Verwachsungen. Akademie-Verlag GmbH, Berlin, p. 875.

Sahlström, F., Jonsson, E., Luth, S., Högdahl, K., Landström, E., Sädbom, S., Lynch, E., Ghaderidosst, S., 2019. Textural evolution of the Lovisa Zn-Pb-(Ag) deposit, Bergslagen, Sweden: Insights from microscopy and 3D X-ray tomography. In: Proceedings 15th SGA Biennial Meeting 2019 Glasgow, Scotland, pp. 443–446.

Selkman, S.O., 1984. A deformation study at the Saxberget sulfide deposit, Sweden. Geol. Fören. Stock. Förh. 106, 235–244. https://doi.org/10.1080/11035898509454641.

Spry, P.G., Plimer, I.R., Teale, G.S., 2008. Did the giant Broken Hill (Australia) Zn–Pb–Ag deposit melt? Ore Geol. Rev. 34, 223–241. https://doi.org/10.1016/j.oregeorev.2007.11.001.

Stephens, M.B., Ripa, M., Lundström, I., Persson, L., Bergman, T., Ahl, M., Wahlgren, C.-H., Persson, P.-O., Wickström, L., 2009. Synthesis of the bedrock geology in the Berslagen region, Fennoscandian Shield, south-central Sweden. Geological Survey of Sweden Ba 58, 1–259.

Stephens, M.B., Andersson, J., 2015. Migmatization related to mafic underplating and intra- or back-arc spreading above a subduction boundary in a 2.0-1.8Ga accretionary orogen. Sweden. Precambrian Res. 264, 235–257. https://doi.org/10.1016/j.precamres.2015.04.019.

Stephens, M.B., Jansson, N.F., 2020. Paleoproterozoic (1.9-1.8 Ga) syn-orogenic magmatism, sedimentation and mineralization in the Bergslagen lithotectonic unit, Svecokarelian orogen, in: Stephens, M.B., Weihed, J.B. (Eds.), Sweden: Lithotectonic Framework, Tectonic Evolution and Mineral Resources. Geological Society Memoir No. 50, pp. 155–206.

Sylvester, P.J., Cabri, L.J., Tubrett, M.N., McMahon, G., Laflamme, J.H.G., Peregoedova, A., 2005. Synthesis and evaluation of a fused pyrrhotite standard reference material for platinum group element and gold analysis by laser ablation-ICPMS. 10th International Platinum Symposium, Oulu, Geological Survey of Finland, Extended abstracts, 16–20.

Tajeddin, H.A., Rastad, E., Yaghoubpour, A., Maghfouri, S., Peter, J.M., Goldfarb, R., Mohajjel, M., 2019. The Barika gold-bearing Kuroko-type volcanogenic massive sulfide (VMS) deposit, Sanandaj-Sirjan zone. Iran. Ore Geol. Rev. 113, 103081. https://doi.org/10.1016/j.oregeorev.2019.103081.

Tiu, G., Jansson, N., Wanhainen, C., Ghorbani, Y., Lilja, L., 2021. Ore mineralogy and trace element (re)distribution at the metamorphosed Lappberget Zn-Pb-Ag-(Cu-Au) deposit, Garpenberg. Sweden. Ore Geol. Rev. 135, 104223. https://doi.org/10.1016/j.oregeorev.2021.104223.

Tomkins, A.G., Frost, B.R., Pattison, D.R.M., 2006. Arsenopyrite melting during metamorphism of sulphide ore deposits. Can. Mineral. 44, 1045–1062. https://doi.org/10.2113/gscanmin.44.5.1045.

Tomkins, A.G., Pattison, D.R.M., Frost, B.R., 2007. On the initiation of metamorphic sulphide anatexis. J. Petrol. 48, 511–535. https://doi.org/10.1093/petrology/egl070.

Vivallo, W., 1984. The geology and origin of the Zn-Pb-Cu sulphide deposit Garpenberg. Meddelanden från Stockholms Universitets Geologiska Institution 257, 222 pp.

Vokes, F., 1969. A review of the metamorphism of sulphide deposits. Earth Sci. Rev. 5, 99–143. https://doi.org/10.1016/0012-8252(69)90080-4.

Vokes, F.M., 1973. Ball texture in sulphide ores. Geol. Fören. Stock. Förh. 95, 403–406. https://doi.org/10.1080/11035897309454251.

Vokes, F.M., Craig, J.R., 1993. Post-recrystallisation Phenomena in metamorphosed stratabound sulphide Ores. Mineral. Mag. 57, 19–28. https://doi.org/10.1180/minmag.1994.058.392.14.

Wagner, T., Jonsson, E., Boyce, A.J., 2005. Metamorphic ore remobilization in the Hällefors district, Bergslagen, Sweden: Constraints from mineralogical and small-scale sulphur isotope studies. Miner. Depos. 40, 100–114. https://doi.org/10.1007/s00126-005-0463-2.

Wagner, T., Klemd, R., Wenzel, T., Mattsson, B., 2007. Gold upgrading in metamorphosed massive sulfide ore deposits: Direct evidence from laser-ablation-inductively coupled plasma-mass spectrometry analysis of invisible gold. Geology 35, 775–778. https://doi.org/10.1130/G23739A.1.

Weihed, Pär, Arndt, N., Billström, K., Duchesne, J.-C., Eilu, P., Martinsson, O., Papunen, H., Lahtinen, R., 2005. 8: Precambrian geodynamics and ore formation: The Fennoscandian Shield. Ore Geol. Rev. 27, 273–322. https://doi.org/10.1016/j.oregeorev.2005.07.008.

Wilson, S.A., Ridley, W.I., Koenig, A.E., 2002. Development of sulfide calibration standards for the laser ablation inductively-coupled plasma mass spectrometry technique. J. Anal. At. Spectrom. 17, 406–409. https://doi.org/10.1039/B108787H.

Yang, Q.C., Jochum, K.P., Stoll, B., Weis, U., Kuzmin, D., Wiedenbeck, M., Traub, H., Andreae, M.O., 2012. BAM-S005 Type A and B: New silicate reference glasses for microanalysis. Geostand. Geoanalytical Res. 36, 301–313. https://doi.org/10.1111/j.1751-908X.2012.00171.x.

Yu, P.-P., Zheng, Y., Wang, C.-M., 2020. Trace elemental and sulfur-lead isotopic variations in metamorphosed volcanogenic massive sulfide (VMS) mineralization systems: An example from the Keketale Pb-Zn(-Ag) deposit, NW China. Ore Geol. Rev. 125, 103685. https://doi.org/10.1016/j.oregeorev.2020.103685.

Zack, T., Hogmalm, K.J., 2016. Laser ablation Rb/Sr dating by online chemical separation of Rb and Sr in an oxygen-filled reaction cell. Chem. Geol. 437, 120–133. https://doi.org/10.1016/j.chemgeo.2016.05.027.

Zakrzewski, M.A., Burke, E.A.J., Kieft, C., 1986. Mineralogical investigations on the Lovisa ore deposit, Bergslagen. Unpublished report, Vrije Universiteit., Amsterdam. p. 14.

Zhao, Z., Wei, J., Liang, S., Gao, T., 2021. Sulfide remobilization and trace element redistribution during metamorphism and deformation at the Xitieshan Pb-Zn deposit, NW China. Ore Geol. Rev. 136, 104170. https://doi.org/10.1016/j.oregeorev.2021.104170.